International Communications in Heat and Mass Transfer 178 (2026) 111615

Contents lists available at ScienceDirect

International Communications in Heat and Mass Transfer

journal homepage: www.elsevier.com/locate/ichmt

Economically advantageous two-Stage Heat Exchanger Configuration for High-Temperature Exhaust Heat Management in Multi-Generation System Utilized in Heat-Driven Humidification-Dehumidification Desalination Unit and sCO_2 Cycle Leveraging Metaheuristic Bat Algorithm

Yonghui Li [a], Ali Basem [b], Hyder H. Abed Balla [c,*], Mohamed Arbi Khlifi [d,**], Haibo Zhang [a,***], Hanaa Abu-Zinadah [e], Zainab Ali Bu sinnah [f], Muyassar Norberdiyeva [g], Yasser Fouad [h,****], Ibrahim Mahariq [i,j,k,*****]

[a] *School of Digital Economy and Management, Sichuan University of Technology and Business, Meishan, Sichuan 620000, China*
[b] *Advanced Technical College, University of Warith Al-Anbiyaa, Karbala, Iraq*
[c] *Aeronautical Technical department, Najaf Technical Institute,Al Furat Al Awsat Technical University, Kufa, Najaf, Iraq*
[d] *Department of Electrical Engineering, Faculty of Engineering, Islamic University of Madinah, Madinah 42351, Saudi Arabia.*
[e] *Department of Mathematics and Statistics, College of science, University of Jeddah, Jeddah, Saudi Arabia.*
[f] *Department of Science and Technology, University Colleges at Nairiyah, University of Hafr Albatin (UHB), Nairiyah 31981, Saudi Arabia*
[g] *Department of Chemistry and Its Teaching Methods, National Pedagogical University of Uzbekistan, Tashkent, Uzbekistan*
[h] *Department of Applied Mechanical Engineering, College of Applied Engineering, Muzahimiyah Branch, King Saud University, P.O. Box 800, Riyadh 11421, Saudi Arabia*
[i] *Department of Electrical and Electronic Engineering, Faculty of Engineering and Architecture, Istanbul Gelisim University, Avcılar- Istanbul, 34310, Istanbul, Türkiye*
[j] *Department of Medical Research, China Medical University Hospital, China Medical University, Taichung, Taiwan*
[k] *University College, Korea University, Seoul 02481, South Korea*

ARTICLE INFO

Keywords:
Thermal management
Heat recovery
Heat-driven HDH desalination
Gas turbine
Metaheuristic bat algorithm
Cost-effective framework

ABSTRACT

This study proposes value-oriented thermal management in a sustainable biomass-based freshwater and hydrogen production system integrating a humidification–dehumidification (HDH) desalination unit with a supercritical CO_2 Brayton cycle and PEM water electrolysis, driven by rice straw biomass. A comprehensive thermodynamic model evaluates system performance, with particular emphasis on freshwater generation under varying operating conditions, including gas turbine pressure ratio, turbine inlet temperature, and biomass feed rate. High-temperature exhaust gases from the gas turbine transfer their thermal energy through two heat exchangers as a cost-effective approach. The first heat exchanger supplies heat to drive the supercritical CO_2 (sCO_2) Brayton cycle, generating additional power. Within the sCO_2 cycle, an internal heat exchanger provides heated air for residential space-heating applications. The second heat exchanger recovers residual exhaust heat to drive the HDH desalination cycle, producing freshwater. The system simultaneously delivers electricity, freshwater, hot air, hydrogen, and oxygen. Performance analyses indicate that increasing the gas turbine pressure ratio enhances electrical power and hydrogen production while reducing thermal outputs such as freshwater and hot air. Conversely, higher turbine inlet temperatures favor freshwater and hot air generation. Results show that freshwater production increases significantly with higher turbine inlet temperature and biomass feed rate, reaching up to 216.8 L/h and 235.3 L/h, while higher pressure ratios reduce water yield due to enhanced energy

* Corresponding author: Aeronautical Technical department, Najaf Technical Institute, Al Furat Al Awsat Technical University, Kufa, Najaf, Iraq.
** Corresponding author: Department of Electrical Engineering, Faculty of Engineering, Islamic University of Madinah, Madinah 42351, Saudi Arabia.
*** Corresponding author: School of Digital Economy and Management, Sichuan University of Technology and Business, Meishan, Sichuan 620000, China
**** Corresponding author: Department of Applied Mechanical Engineering, College of Applied Engineering, Muzahimiyah Branch, King Saud University, P.O. Box 800, Riyadh 11421, Saudi Arabia
***** Corresponding author at: Department of Electrical and Electronic Engineering, Faculty of Engineering and Architecture, Istanbul Gelisim University, Avcılar-Istanbul, 34310, Istanbul, Türkiye
E-mail addresses: hyderballa@atu.edu.iq (H.H. Abed Balla), medarbi@iu.edu.sa (M.A. Khlifi), SCI868@126.com (H. Zhang), yfouad@ksu.edu.sa (Y. Fouad), ibmahariq@gmail.com (I. Mahariq).

https://doi.org/10.1016/j.icheatmasstransfer.2026.111615

Available online 1 June 2026

extraction in the power cycle. A metaheuristic bat algorithm is used for multi-objective optimization to maximize freshwater and hydrogen production while improving overall system efficiency. An optimal configuration achieves high freshwater yield, considerable hydrogen generation, and efficiency exceeding 80%.

1. Introduction

The rapid growth of global energy demand, coupled with increasing environmental concerns, has intensified the search for sustainable and efficient energy systems [1–3]. Conventional fossil-fuel-based power generation not only depletes natural resources but also significantly contributes to greenhouse gas emissions and environmental degradation. In this context, multi-generation energy systems [4–6] have emerged as a promising approach, offering the simultaneous production of electricity, heat, freshwater, and chemical fuels such as hydrogen [7–9]. These systems aim to enhance overall efficiency by utilizing energy streams more effectively and integrating renewable or alternative energy sources, thereby reducing environmental impact and improving energy security [10,11].

Among renewable options, biomass-based energy systems [12,13] are particularly attractive due to their carbon-neutral nature and wide availability, especially from agricultural residues such as rice straw, wood chips, and other lignocellulosic materials [14–16]. Integrating biomass with advanced thermodynamic cycles, including supercritical carbon dioxide (sCO_2) Brayton cycles, electrochemical hydrogen production, and humidification–dehumidification (HDH) desalination, enables efficient use of fuel energy while producing multiple valuable outputs. Modern high-efficiency recuperation concepts for gas turbines, including chemically recuperated and exhaust-driven fuel-reforming systems, have shown strong potential for improving cycle performance [17,18]. Biomass-based hydrogen plays a key role in enabling clean and sustainable energy systems [19–21]. The design and optimization of such integrated systems are essential for maximizing energy utilization, reducing emissions, and providing sustainable solutions for both rural and industrial applications. Consequently, research in this domain addresses both technical challenges and environmental imperatives, making it a critical area for advancing next-generation energy technologies.

Sharifishourabi et al. [22] developed a solar-biomass-based multigeneration system integrating Brayton, Rankine, and absorption cycles to produce heat, power, hydrogen, and hot water. The system demonstrated notable energy (58.43%) and exergy (56.92%) efficiencies, highlighting the feasibility of combining renewable sources and advanced thermodynamic cycles for efficient, multi-output energy systems, aligning with the objectives of the present study. Fu et al. [23] proposed a biomass gasification-based fuel cell trigeneration system with an exergy-cost-carbon approach, integrating ORC, absorption, and heat exchange cycles. The study provided comprehensive insights into cost, carbon footprint, and exergy relationships for multiple energy outputs, demonstrating how optimized configuration and exergy-level analysis enhance the performance and sustainability of multigeneration systems. Xu et al. [24] introduced a polygeneration system converting lignocellulosic biomass (corn stover) into dimethyl ether (DME) and electricity using S-CO_2 Brayton and WGS cycles. The system achieved 49.54% energy efficiency and 41.12% exergy efficiency, while capturing CO_2, highlighting the potential of integrating biomass conversion and advanced cycles for simultaneous fuel and power production. Chen et al. [25] presented an innovative biomass-based multigeneration system producing power, freshwater, cooling, and hydrogen. The integration of supercritical CO_2 cycles, HDH desalination, and electrolyzers demonstrated efficient multi-energy utilization. Parametric and hybrid optimization studies revealed trade-offs between exergy efficiency and resource outputs, emphasizing the importance of multi-objective optimization for sustainable energy solutions. Li et al. [26] designed an integrated biomass-to-energy system combining gasification and pyrolysis for electricity and hydrogen production. Results showed high energy efficiency, lower CO_2 intensity, and the influence of pyrolysis and gasification temperatures on hydrogen and power outputs. This study reinforces the value of hybrid thermochemical processes in achieving efficient, environmentally-friendly biomass utilization. Ju et al. [27] developed a biomass-powered micro energy grid (BSP-MEG) for islands, integrating desalination and power-to-hydrogen. Using hybrid differential evolution, the system optimized energy, water, and material flows, reduced costs and environmental risks, and enhanced renewable resource utilization, demonstrating effective multi-objective optimization for self-sustainable regional energy systems.

This study addresses the growing demand for efficient, sustainable, and multifunctional energy systems through the integration of biomass-based multigeneration technologies with advanced optimization methods. In contrast to conventional configurations, the proposed system incorporates a supercritical CO_2 Brayton cycle, hydrogen production, freshwater generation, and air heating within a unified and flexible framework. This integrated design enables the simultaneous production of multiple energy carriers while enhancing the overall thermodynamic performance of the system. A major contribution of this work lies in the application of the metaheuristic Bat Algorithm for multi-objective optimization. This approach makes it possible to determine optimal operating conditions that achieve a desirable compromise among power generation, freshwater and hydrogen production, system efficiency, and emissions reduction. The adopted methodology offers a systematic means of investigating the complex and nonlinear interactions among key operating parameters, including pressure ratio, turbine inlet temperature, and biomass feed rate. The objectives of this research are threefold: (i) to assess the thermodynamic and environmental performance of the proposed biomass-based polygeneration system under a range of operating conditions; (ii) to optimize system performance using the Bat Algorithm and identify the most promising operating points for practical application; and (iii) to compare the system outputs with those reported in the literature in order to demonstrate potential improvements in efficiency, sustainability, and energy utilization. The results of this study are expected to support the development of next-generation renewable energy systems that are environmentally responsible, operationally efficient, and economically feasible.

2. System description and modeling

2.1. System description

The proposed multi-generation energy system (proposed in Fig. 1) utilizes rice straw biomass as the primary fuel for a gas turbine unit. The biomass and air are fed into the turbine combustor, where combustion reactions occur to generate power. A portion of this electrical power constitutes the first share of the system's output, while another portion drives a proton exchange membrane (PEM) electrolyzer to produce hydrogen and oxygen from water electrolysis. The generated gases are subsequently stored as hydrogen and oxygen reserves. The high-temperature exhaust gases leaving the gas turbine transfer their thermal energy through two heat exchangers. The first exchanger supplies the necessary heat to operate a supercritical carbon dioxide (sCO_2) Brayton cycle, which generates an additional portion of power, contributing to the second segment of the total power output. Within the sCO_2 Brayton cycle, an internal heat exchanger also provides heated air for residential space-heating applications. The second heat exchanger recovers residual exhaust heat to drive a humidification–dehumidification (HDH) desalination cycle, thereby producing freshwater. Ultimately, the remaining flue gases are released as emissions. Hence, the system simultaneously delivers electricity, freshwater, hot air, hydrogen storage, and oxygen storage. The overall efficiency and emission levels are analyzed as key performance indicators.

2.2. System modeling

When formulating the thermodynamic model, radiative heat transfer within the system components is neglected and all working fluids are assumed to behave as ideal gases [28,29]. The model is developed under steady-state operation with thermodynamic equilibrium assumed throughout all components [30,31]; changes in kinetic and potential energy are neglected [32,33]. Ambient reference conditions are taken as 1 bar and 25 °C. It should be noted that the assumptions of complete combustion and ideal gas behavior may introduce minor deviations in the predicted thermodynamic properties; however, these assumptions are commonly adopted for system-level performance evaluation and are not expected to significantly affect the comparative trends or the overall conclusions of the present study.

Fuel is supplied to the combustion chamber and reacts with the air stream under predefined operating conditions. The outlet stream of the combustion chamber consists of nitrogen, carbon dioxide, steam, and oxygen, assuming a complete combustion process. Because complete oxidation is assumed, formation of dioxins and furans is neglected. The global combustion reaction between the fuel and the air agent is expressed as [34]:

$$\dot{n}_{fuel}CO_{x_1}H_{x_2}N_{x_3} + \dot{n}_{air} \rightarrow \dot{n}_{N_2}N_2 + \dot{n}_{CO_2}CO_2 + \dot{n}_{H_2O}H_2O + \dot{n}_{O_2}O_2 \quad (1)$$

where $\dot{n}_{fuel}$ and $\dot{n}_{air}$ are the molar flow rates of the fuel and air, respectively. x_1, x_2, and x_3 represent the numbers of oxygen, hydrogen, and nitrogen atoms per mole of carbon in the fuel.

The molar flow rate of each exhaust component $\dot{n}_i$ is determined from elemental balances:

$$\dot{n}_{fuel}x_3 + \dot{n}_{air}(N\ of\ air) = 2\dot{n}_{N_2} \quad (2)$$

$$\dot{n}_{fuel} = \dot{n}_{CO_2} \quad (3)$$

$$\dot{n}_{fuel}x_2 = 2\dot{n}_{H_2O} \quad (4)$$

$$\dot{n}_{fuel}x_1 + \dot{n}_{air}(O\ of\ air) = 2\dot{n}_{CO_2} + \dot{n}_{H_2O} + 2\dot{n}_{O_2} \quad (5)$$

The combustion energy balance is defined as:

$$\dot{n}_{fuel}\overline{h}_{fuel} + \dot{n}_{air}\overline{h}_{air} \rightarrow \dot{n}_{N_2}\overline{h}_{N_2} + \dot{n}_{CO_2}\overline{h}_{CO_2} + \dot{n}_{H_2O}\overline{h}_{H_2O} + \dot{n}_{O_2}\overline{h}_{O_2} \quad (6)$$

Rice straw biomass has been selected as the fuel for the combustion chamber [35]. Its proximate composition consists of 16.55 wt% fixed carbon, 65.23 wt% volatile matter, 5.58 wt% moisture, and 12.64 wt% ash. The ultimate analysis reveals 38.61 wt% carbon, 4.28 wt% hydrogen, 1.08 wt% nitrogen, and 37.16 wt% oxygen. The lower heating value (LHV) of the rice straw biomass is 14.4 MJ/kg, indicating a moderate energy density typical of agricultural residues [35].

Water electrolysis has been widely studied as a promising technique for hydrogen production [36–38]. In this process, water is decomposed into hydrogen and oxygen gases through the application of an electric current, as expressed by the following reaction [39–41]:

$$\mathrm{H_2O_{(l)} \rightarrow H_{2(g)} + \frac{1}{2}O_{2(g)}} \quad (7)$$

The corresponding reduction and oxidation reactions are formulated as [42,43]:

$$\mathrm{2H_2O_{(l)} + 2e^- \rightarrow H_{2(g)} + 2OH^-{}_{(aq)}} \quad (8)$$

$$\mathrm{H_2O_{(l)} \rightarrow \frac{1}{2}O_{2(g)} + 2H^+{}_{(aq)} + 2e^-} \quad (9)$$

The chemical reaction occurring within the mixing chamber is represented by [44,45]:

$$\mathrm{2H^+{}_{(aq)} + 2OH^-{}_{(aq)} \rightarrow 2H_2O_{(l)}} \quad (10)$$

The molar flow rate of the produced hydrogen is calculated by [46]:

$$\dot{n}_{H_2,out} = \frac{J}{2F} \quad (11)$$

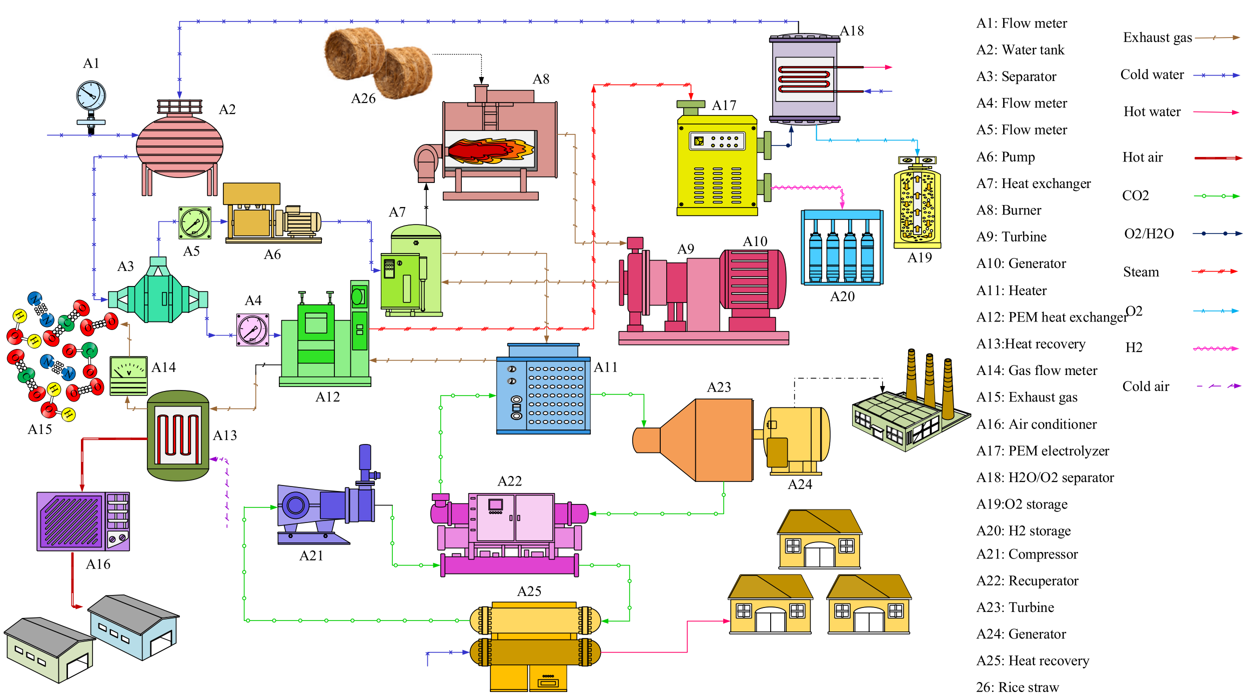

Fig. 1. Schematic representation of the proposed integrated energy system illustrating the main components and thermodynamic interactions among the subsystems.

where J is the current density and F denotes the Faraday constant. The outlet water and oxygen flow rates are defined as [46]:

$$\dot{n}_{H_2O,out} = \dot{n}_{H_2O,in} - \frac{J}{2F} \tag{12}$$

$$\dot{n}_{O_2,out} = \frac{J}{4F} \tag{13}$$

The input power supplied to the electrolyzer can be evaluated by [47,48]:

$$\dot{W}_{PEM} = ANVJ \tag{14}$$

where A is the active surface area, N represents the cell number, and V is the cell voltage, calculated as [49]:

$$V = V_{act} + V_{ohm} + V_N \tag{15}$$

The activation, ohmic, and Nernst voltages are respectively defined as [49]:

$$V_{act} = \frac{\overline{R}T}{F}\left(sinh^{-1}\left(\frac{J}{2J_{o,an}}\right) + sinh^{-1}\left(\frac{J}{2J_{o,ca}}\right)\right) \tag{16}$$

$$V_{ohm} = J \times \int_0^D \frac{dx}{\Gamma_{PEM}[\xi(x)]} \tag{17}$$

$$V_N = 1.229 - 8.5 \times 10^{-4} \times (T_{PEM} - 298) \tag{18}$$

The local membrane conductivity is expressed as [49]:

$$\Gamma_{PEM}[\zeta(x)] = (0.5136 \times \zeta(x) - 0.326) \times e^{1268\times\left(\frac{1}{303}-\frac{1}{T_{PEM}}\right)} \tag{19}$$

where

$$\zeta(x) = \left(\frac{\zeta_{an} - \zeta_{ca}}{D}\right)x + \zeta_{ca} \tag{20}$$

Finally, the exchange current densities for the anode and cathode are given as [50,51]:

$$J_{o,an} = J_{an}^{ref} e^{-\frac{E_{act,an}}{\overline{R}T_{PEM}}} \tag{21}$$

$$J_{o,ca} = J_{ca}^{ref} e^{-\frac{E_{act,ca}}{\overline{R}T_{PEM}}} \tag{22}$$

In recent years, supercritical carbon dioxide (sCO_2) has been widely investigated as a working fluid for Brayton cycles due to its high thermal efficiency, low environmental impact, and non-toxic characteristics [52–54]. The sCO_2 subsystem considered in this study is a simple recuperated Brayton cycle, in which the recuperator is used to recover heat from the turbine exhaust and preheat the compressed working fluid before entering the heater. The power outputs of the compressor and turbine and their respective isentropic efficiencies are defined as [55–57]:

$$P_{com} = \Delta h_{com} \dot{m}_{CO_2} \tag{23}$$

$$P_{tur} = \Delta h_{tur} \dot{m}_{CO_2} \tag{24}$$

$$\eta_{com} = \frac{\Delta h_{com}^s}{\Delta h_{com}} \tag{25}$$

$$\eta_{tur} = \frac{\Delta h_{tur}}{\Delta h_{tur}^s} \tag{26}$$

Here, Δh denotes the enthalpy difference between outlet and inlet, and Δh^s represents the isentropic enthalpy change. The heat transferred in a heat exchanger is expressed as [58–60]:

$$Q_{HE} = \dot{m}_{CO_2}\left(\Delta h^{hot}\right) \tag{27}$$

where Δh^{hot} is the enthalpy change of the hot stream. The efficiency of the heat exchanger is defined as [61,62]:

$$\eta_{HE} = \frac{\Delta h^{hot}}{\Delta h^{cold}} \tag{28}$$

with Δh^{cold} representing the enthalpy difference in the cold stream.

Humidification-dehumidification (HDH) desalination couples an air-driven humidifier with a dehumidifier to extract fresh water from saline feed [63–66]. Mass production of freshwater in the dehumidifier is obtained from the change in the air humidity ratio across that component [67]:

$$\dot{m}_f = \dot{m}_a \alpha_{in} - \dot{m}_a \alpha_{out}) \tag{29}$$

In the humidifier, the freshwater yield may be expressed similarly, and is also equal to the difference between the seawater feed and the brine discharge [48,68]:

$$\dot{m}_f = \dot{m}_a \alpha_{out} - \dot{m}_a \alpha_{in} = \dot{m}_s - \dot{m}_b \tag{30}$$

Energy conservation is applied separately on the dehumidifier and the humidifier. For the dehumidifier:

$$\dot{m}_s \Delta h_s = \dot{m}_a \Delta h_a - \dot{m}_f h_f \tag{31}$$

and for the humidifier:

$$\dot{m}_s h_s = \dot{m}_a \Delta h_a + \dot{m}_b h_b \tag{32}$$

Here $\dot{m}$ denotes mass flow (kg/s), α is humidity ratio (kg water per kg dry air), h specific enthalpy (kJ/kg), and Δh indicates the enthalpy difference between inlet and outlet of the corresponding stream.

Based on a preliminary screening analysis, pressure ratio (5–15), turbine inlet temperature (800–1000 °C), and biomass feed rate (1.25–1.75 kg/min) are selected as the main decision variables affecting the system performance.

2.3. Metaheuristic bat algorithm

In this study, the bat algorithm, a nature-inspired metaheuristic optimization technique [69], is employed to determine the optimal operating conditions of the integrated multi-generation energy system. Fig. 2 presents the flowchart of the bat algorithm, outlining the sequential steps of the optimization process from initialization of the bat population to iterative updating of candidate solutions and convergence toward the optimal solution. The algorithm is inspired by the echolocation behavior of microbats, which use sound pulses to navigate and locate prey [70,71]. Each bat in the algorithm represents a candidate solution, defined by a set of decision variables including pressure ratio, turbine inlet temperature, and rice straw feed rate. The movement of bats through the search space is governed by velocity and position updates, with adjustments in loudness and pulse emission rate controlling the exploration and exploitation balance [72,73]. Bats with higher fitness, evaluated based on a multi-objective function incorporating power output, hydrogen and oxygen production, freshwater generation, system efficiency, and emissions, are more likely to influence the swarm's trajectory toward promising regions of the solution space. The algorithm iteratively updates the positions and velocities of bats, adapting the pulse frequency and emission rate to refine the search for optimal solutions [74]. This approach effectively navigates the high-dimensional, nonlinear, and multi-modal landscape of the system, enabling identification of multiple candidate optimum points that balance energy, water, and hydrogen outputs while minimizing emissions. The flexibility, simplicity, and proven convergence properties of the bat algorithm make it particularly suitable for complex multi-objective optimization in advanced energy systems [75].

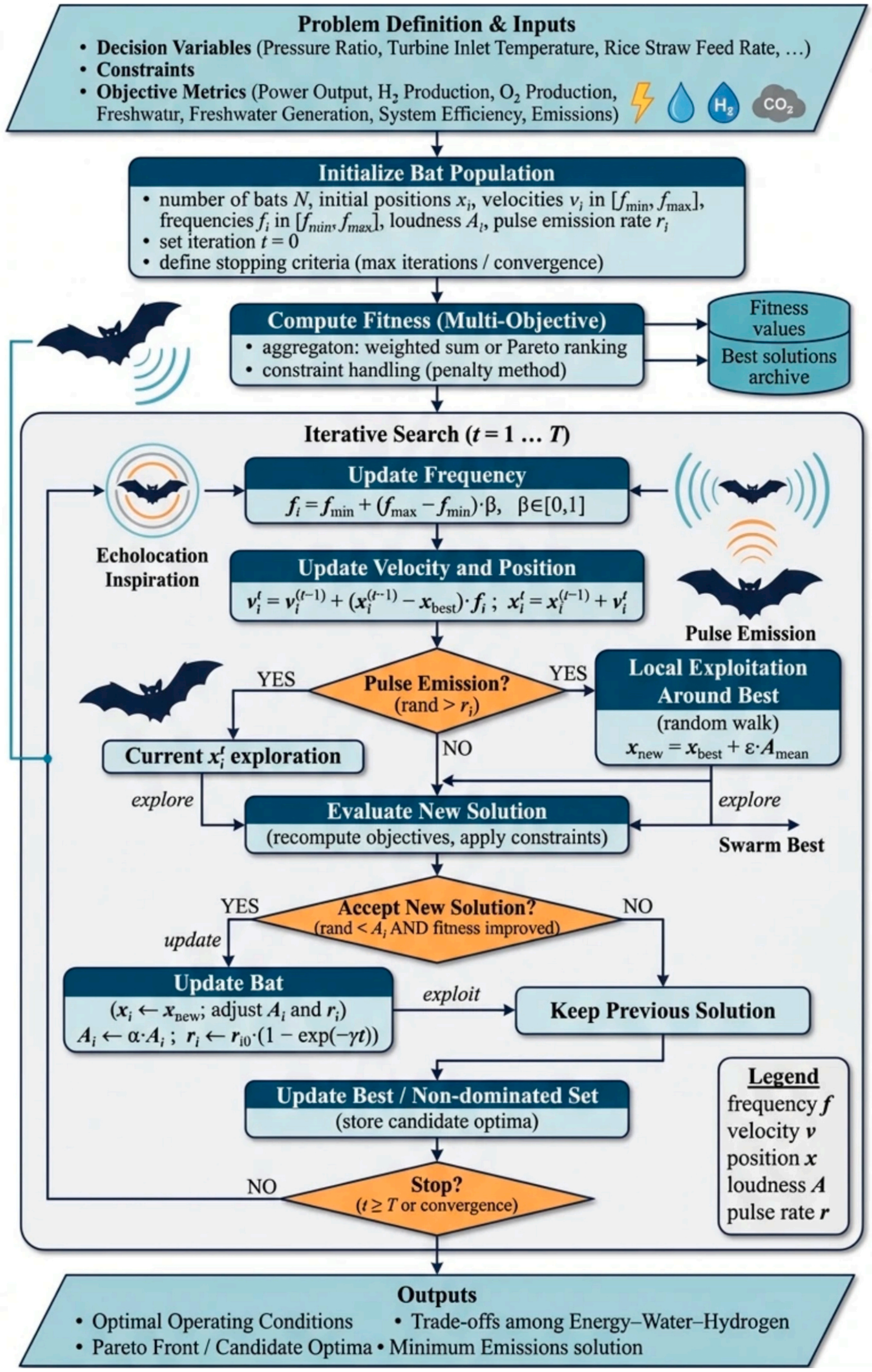

Fig. 2. Flowchart of the metaheuristic bat algorithm illustrating the main optimization procedure, including initialization, solution update using frequency, velocity and position adjustments, evaluation of fitness, and the acceptance criteria based on loudness and pulse emission rate.

3. Results and discussion

3.1. Model validation

As shown in Fig. 3, the HDH thermodynamic model was tested against the results reported in [76] for both temperature and flow variables. Maximum absolute deviations for the dehumidifier and product-water temperatures were under 3%, and the discrepancies for seawater and distilled-water mass flow rates were under 2%. These validation outcomes indicate the model is both accurate and dependable.

In Fig. 4, the cell voltage predictions produced by the PEM model are benchmarked against the experimental/literature curves from references [77,78] at multiple current densities. The comparison yields a high-quality fit: modeled potentials align with the references through the examined current range, with only marginal differences at isolated points. This close conformity confirms that the model reliably represents electrochemical behavior under practical operating conditions. Accordingly, the validation confirms and validates the PEM modeling approach, establishing confidence in its accuracy for both analysis and design tasks.

To assess the fidelity of the supercritical CO_2 Brayton-cycle model, we examined a matrix of eight operating points. These cases span two

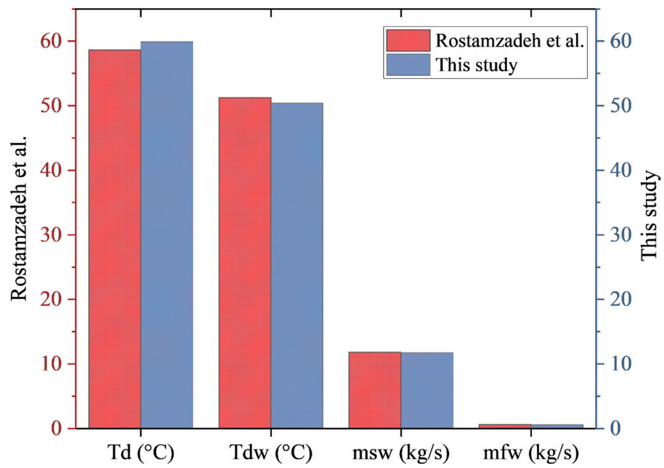

Fig. 3. Validation chart of HDH desalination showing strong agreement between modeled and reference temperatures and mass flow values, verifying the accuracy of the developed model.

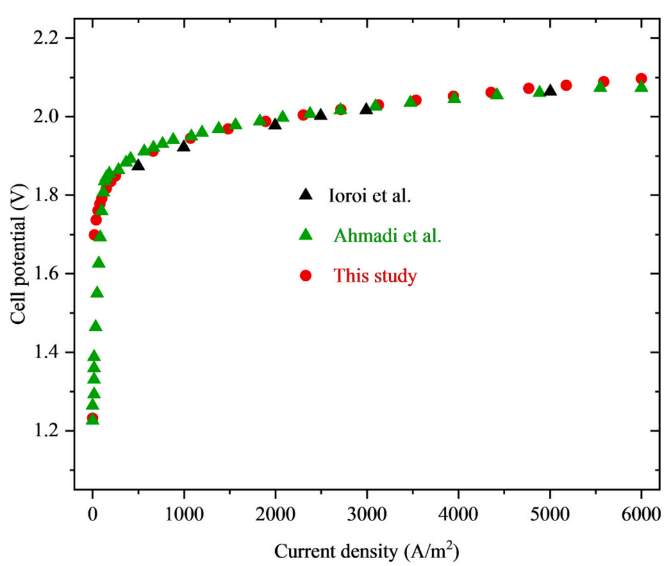

Fig. 4. Validation figure showing the predicted voltage behavior of the PEM cell versus current density in comparison to literature data; results confirm the model's reliability.

maximum pressures (200 and 300 bar), two turbine inlet temperatures (550 and 750 °C) and two ambient/initial temperatures (T1 = 32 °C and 50 °C), reproducing the test conditions used by the reference study [79]. For each condition the computed pressure ratio was extracted and benchmarked against the corresponding values reported in [79]. The comparison, plotted in Fig. 5, shows excellent agreement: the modeled pressure ratios closely follow the reference results across all eight scenarios. Quantitatively, deviations remain below 3% in every case. Taken together, the benchmarking exercise demonstrates that the present thermodynamic model reliably captures the cycle behavior under a broad set of temperatures and pressures, and thus the model's predictive capability for pressure-ratio estimation is validated.

3.2. System performance assessments

Fig. 6 illustrates the influence of the gas turbine pressure ratio (PR) on the overall system performance in terms of total electrical power output, freshwater generation rate, and hot air production capacity. The results reveal opposite trends among these three outputs as PR increases from 5 to 15. The total power output rises monotonically with higher PR owing to improved turbine expansion work and enhanced thermal utilization within the sCO_2 Brayton cycle. Specifically, power increases from 198 kW at PR = 5 to 286.5 kW at PR = 15, representing an absolute gain of 88.5 kW and a 44.7% improvement. This growth reflects the combined effect of reduced compressor work and greater turbine-outlet enthalpy drop, which collectively elevate the net power of the hybrid gas turbine/sCO_2 subsystem. Conversely, both freshwater and hot air outputs exhibit declining tendencies with rising PR. The freshwater production rate decreases from 201.7 L/h at PR = 5 to 97.95 L/h at PR = 15; a reduction of 103.75 L/h, corresponding to a 51.4% decline. Similarly, the hot air volumetric flow rate falls from 5588 m^3/h to 3148 m^3/h, amounting to a 43.7% decrease. These reductions stem from the diminished exhaust gas temperature at higher PR, which lowers the available thermal energy transferred through the heat-recovery exchangers to the HDH desalination and space-heating units. Overall, an increase in PR enhances the power generation efficiency of the integrated system but compromises the thermal driven products (freshwater and hot air). Therefore, an optimal PR must balance electrical gain against the reduction in co-generated heat dependent outputs to maximize the system's multi-generation effectiveness. The analysis of power, freshwater, and hot air production with respect to pressure ratio shows consistent trends in line with prior studies. Increasing the pressure ratio enhances power output but reduces freshwater and hot air generation. These trends are consistent with previous investigations by Ibrahim et al. [80], Ghaffarpour et al. [81], Ahmadi et al. [82], and Haseli et al. [83], confirming that higher pressure ratios favor energy conversion while slightly diminishing auxiliary outputs such as desalination and space heating.

Fig. 7 presents the variation of hydrogen and oxygen storage rates with respect to the gas turbine pressure ratio (PR). Both storage outputs exhibit a clear and consistent upward trend as PR increases from 5 to 15. This positive correlation arises because higher PR enhances the overall power output of the integrated system (as shown in Fig. 6), thereby providing more electrical energy to drive the PEM electrolyzer for water electrolysis. The hydrogen storage rate increases from 1.452 kg/h at PR = 5 to 2.101 kg/h at PR = 15, corresponding to an absolute gain of 0.649 kg/h and a 44.7% increase. Similarly, the oxygen storage rate rises from 11.52 kg/h to 16.67 kg/h, resulting in an improvement of 5.15 kg/h or 44.7%. The identical growth percentages confirm the stoichiometric relationship between the two gases in the electrolysis process, in which oxygen production is theoretically eight times that of hydrogen on a mass basis. The monotonic enhancement of both gases with PR reflects the thermodynamic and electrical synergies between the gas turbine, the sCO_2 Brayton cycle, and the PEM electrolyzer. At higher PR, the combined power generation subsystems deliver greater net electrical output, a portion of which is utilized to sustain higher electrolysis current density. Consequently, more water molecules are decomposed per unit time, yielding higher H_2 and O_2 production rates. These findings emphasize that optimizing the gas turbine pressure ratio not only boosts power generation efficiency but also strengthens the hydrogen and oxygen storage capacities, thereby improving the overall multi-generation potential and flexibility of the proposed system.

Fig. 8 illustrates the variation of overall cycle efficiency and emission intensity as a function of the pressure ratio (PR) in the supercritical CO_2 Brayton cycle. The results clearly indicate that increasing the pressure ratio leads to a substantial enhancement in system efficiency while simultaneously reducing emission levels. Specifically, as PR rises from 5 to 15, the efficiency improves continuously from 50.4% to 76.99%, representing an impressive 52.7% relative increase. This improvement can be attributed to the elevated thermodynamic potential of the working fluid at higher compression ratios, which strengthens the recuperation process and reduces irreversibilities across the compressor and turbine. Consequently, a greater portion of the input heat is converted into useful work, leading to improved performance. In contrast, the emission intensity decreases steadily with increasing PR, declining

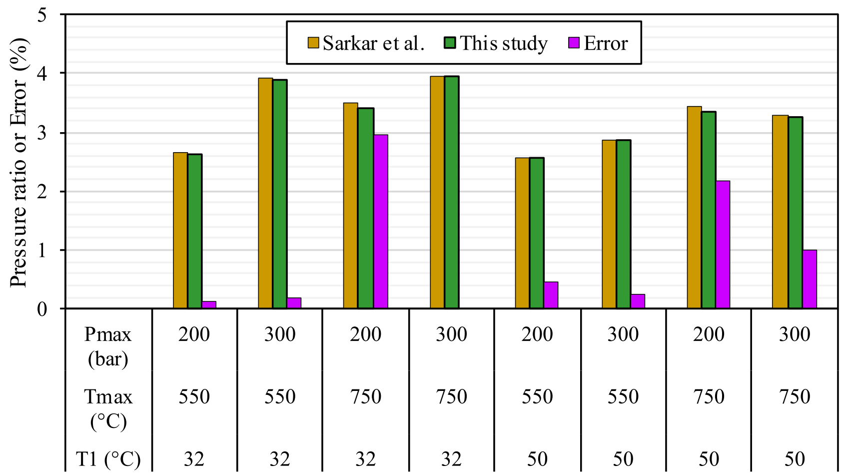

Fig. 5. Comparison between modeled and reference pressure-ratio data for various temperatures and pressures; excellent agreement validates the sCO_2 Brayton cycle model.

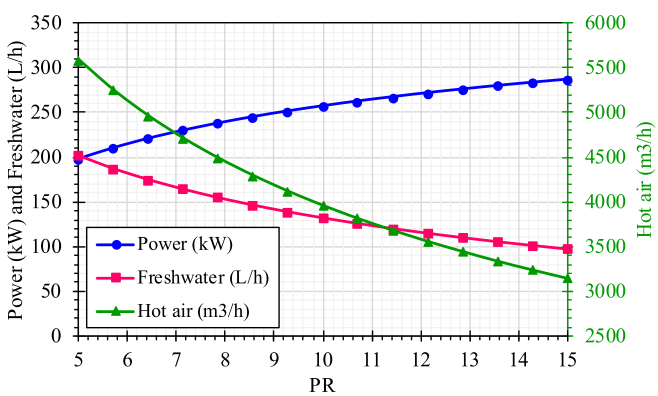

Fig. 6. Variation of total power output, freshwater production rate, and hot air generation with gas turbine pressure ratio (PR). Increasing PR markedly improves power generation (+44.7%) but reduces freshwater (−51.4%) and hot-air (−43.7%) yields.

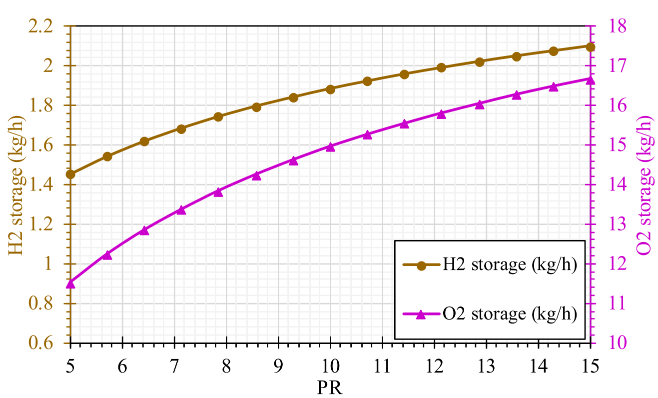

Fig. 7. Effect of gas turbine pressure ratio (PR) on hydrogen and oxygen storage rates. Both H_2 and O_2 outputs increase steadily with rising PR, from 1.452 to 2.101 kg/h and from 11.52 to 16.67 kg/h, respectively, corresponding to a 44.7% enhancement driven by greater electrical power available for electrolysis.

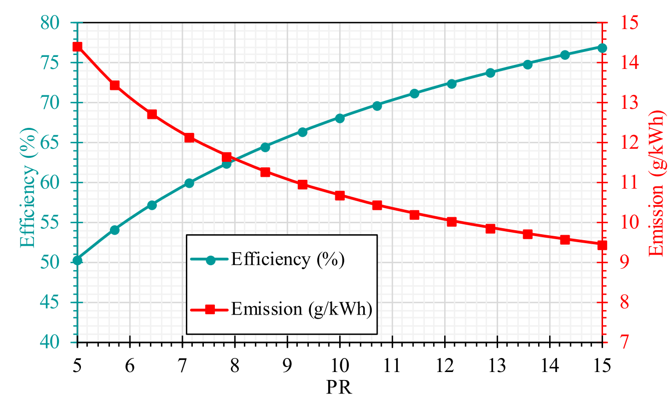

Fig. 8. Variation of overall efficiency and emission intensity with pressure ratio (PR) in the supercritical CO_2 Brayton cycle, showing efficiency improvement from 50.4% to 76.99% and emission reduction from 14.43 g/kWh to 9.446 g/kWh as PR increases from 5 to 15.

from 14.43 g/kWh at PR = 5 to 9.446 g/kWh at PR = 15. This corresponds to a 34.6% reduction in emissions, highlighting the environmental advantages of operating at higher pressure ratios. The reduced emission rate results from enhanced combustion efficiency and better energy conversion, which together lower the specific fuel consumption for the same power output. Additionally, the smoother temperature gradients at higher PR levels contribute to more complete fuel oxidation and lower carbon-based byproducts. The simultaneous increase in efficiency and decrease in emission levels with higher pressure ratios emphasize the dual techno-environmental benefits of system optimization. Thus, selecting a suitably high PR offers a favorable balance between thermodynamic performance and environmental sustainability in the supercritical CO_2 Brayton cycle. These observations align with previous studies by Ebrahimi and Majidi [84], Mojaver et al. [85], Ghaffarpour et al. [81], and Sanjay et al. [86], highlighting the interplay between biomass type, pressure ratio, and environmental performance.

Fig. 9 illustrates the influence of the gas turbine inlet temperature (T) on three key performance parameters: power output, freshwater production rate, and hot air generation within the integrated supercritical CO_2 Brayton-based system. The results reveal a contrasting trend among these outputs as the turbine inlet temperature increases from 800 °C to 1000 °C. Specifically, while the power output exhibits a gradual decline, both freshwater production and hot air generation consistently increase. As temperature rises from 800 °C to 1000 °C, the power output decreases from 281.3 kW to 239.4 kW, corresponding to a 14.9% reduction. This decrease is attributed to the lower density and higher specific volume of the working fluid at elevated temperatures, which reduces the mass flow rate through the turbine and consequently the mechanical power produced consistent with observations by Bakare et al. [87], Ibrahim and

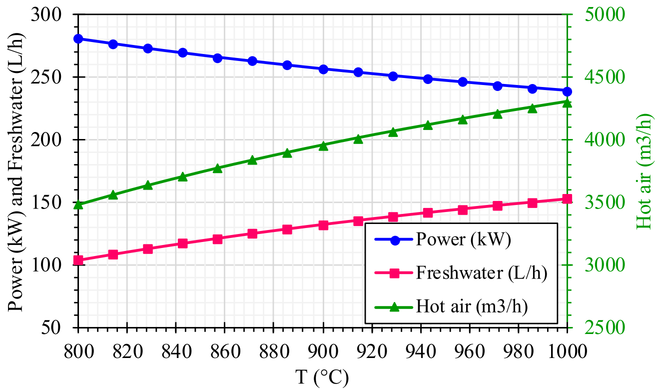

Fig. 9. Variation of power output, freshwater production, and hot air generation with gas turbine inlet temperature, showing a power decrease from 281.3 kW to 239.4 kW (−14.9%), freshwater increase from 104.2 L/h to 153 L/h (+46.8%), and hot air increase from 3490 m^3/h to 4306 m^3/h (+23.4%) as temperature rises from 800 °C to 1000 °C.

Rahman [88], and Ghaffarpour et al. [81]. Despite this decline, the thermal energy available in the exhaust gases becomes more favorable for cogeneration applications. Conversely, the freshwater production rate increases markedly from 104.2 L/h to 153 L/h, representing a 46.8% enhancement corroborating trends reported by Assareh et al. [89] and Ding et al. [90], while the hot air generation rises from 3490 m^3/h to 4306 m^3/h, amounting to a 23.4% increase in agreement with findings of Yilmaz et al. [91] and Mojaver et al. [85]. These upward trends result from the greater availability of waste heat at higher turbine outlet temperatures, which improves the performance of the desalination and air-heating subsystems. The intensified heat transfer processes in both units enable more efficient utilization of the thermal energy that would otherwise be lost. Increasing the turbine inlet temperature leads to a trade-off: a moderate reduction in power output is counterbalanced by significant gains in freshwater and thermal energy production. This outcome underscores the importance of optimizing turbine inlet temperature to achieve the best compromise between power efficiency and multi-generation performance.

Fig. 10 illustrates the effect of gas turbine inlet temperature (T) on the rates of hydrogen and oxygen storage in the integrated hybrid energy system. The results clearly show that both H_2 and O_2 storage capacities decrease steadily as the turbine inlet temperature rises from 800 °C to 1000 °C, indicating a decline in electrolyzer performance with increasing gas turbine temperature. Quantitatively, the H_2 storage rate declines from 2.063 kg/h to 1.756 kg/h, corresponding to a 14.9% reduction, while the O_2 storage rate decreases from 16.38 kg/h to 13.93 kg/h, equivalent to a 15.0% reduction. This behavior is in line with previous investigations by Abid et al. [92] and Hai et al. [93]. These nearly proportional reductions reflect the direct electrochemical relationship between hydrogen and oxygen generation within the water-splitting unit. The observed decline in storage performance can be attributed to the redistribution of available energy within the system. At higher turbine inlet temperatures, a larger portion of the input heat is converted into mechanical work in the gas turbine, leaving comparatively less waste heat available to drive the thermal and electrical processes that power the electrolyzer. Consequently, the reduced electrical energy input to the electrolysis subsystem results in diminished rates of hydrogen and oxygen production.

Fig. 11 presents the influence of the gas turbine inlet temperature (T) on the overall system efficiency and emission intensity. The results demonstrate that as the turbine inlet temperature increases from 800 °C to 1000 °C, system efficiency decreases progressively, while emission levels increase correspondingly. This inverse trend highlights the thermal and environmental trade-offs associated with high-temperature turbine operation within the integrated Brayton-based multi-generation system. Specifically, the system efficiency declines from 75.28% to 62.96%, representing a 16.4% reduction, whereas the emission intensity rises from 9.66 g/kWh to 11.55 g/kWh, corresponding to a 19.6% increase. These trends agree with earlier studies by Bakare et al. [87], Haseli et al. [83], and Ebrahimi and Majidi [84], highlighting the inverse relationship between thermal loading and overall thermodynamic performance. The reduction in efficiency is primarily due to the diminishing performance of subsystems such as the electrolyzer and desalination units at elevated temperatures. As the turbine inlet temperature rises, a greater portion of the input thermal energy is converted into high-grade work within the gas turbine, leaving less residual heat available for low-temperature processes, thereby reducing the overall energy recovery efficiency. The observed increase in emissions is linked to higher fuel consumption needed to sustain elevated turbine inlet temperatures. Although the power output of the system decreases only moderately, the higher combustion temperature results in greater CO_2 release per unit of net energy generated. Consequently, optimizing turbine temperature becomes crucial not only for energy efficiency but also for environmental sustainability.

Fig. 12 illustrates the impact of the rice straw feed rate on three primary performance indicators of the integrated system: power generation, freshwater production, and hot air output. As the feed rate of rice straw increases from 1.25 kg/min to 1.75 kg/min, all three parameters exhibit a consistent upward trend, demonstrating the strong dependency of system productivity on the amount of biomass supplied to the gasification and combustion units. The power output rises from 214.1 kW to 299.8 kW, corresponding to a 40.1% increase, while

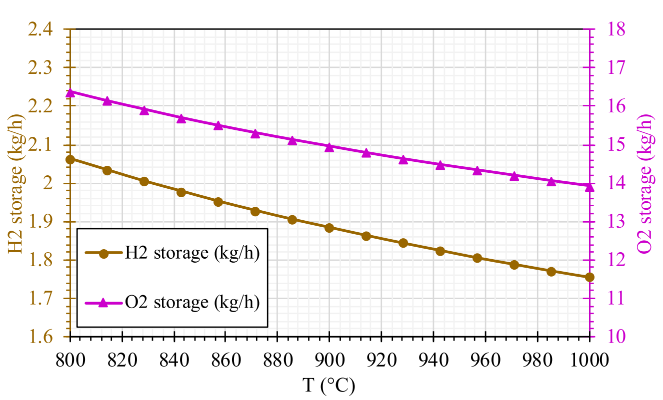

Fig. 10. Variation of hydrogen and oxygen storage rates with gas turbine inlet temperature, showing a decrease in H_2 storage from 2.063 to 1.756 kg/h (−14.9%) and O_2 storage from 16.38 to 13.93 kg/h (−15.0%) as temperature increases from 800 °C to 1000 °C.

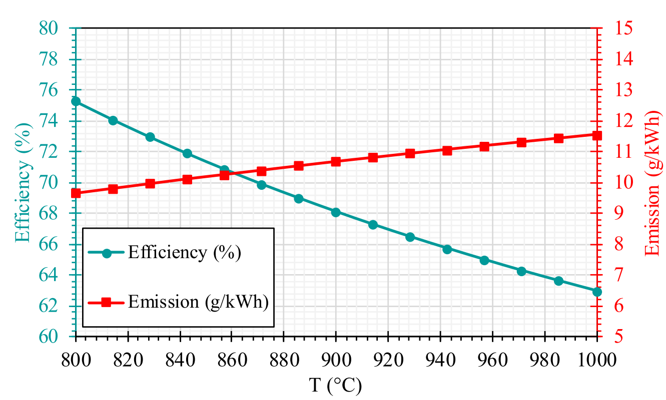

Fig. 11. Variation of system efficiency and emission intensity with gas turbine inlet temperature, showing a decrease in efficiency from 75.28% to 62.96% (−16.4%) and an increase in emissions from 9.66 g/kWh to 11.55 g/kWh (+19.6%) as temperature rises from 800 °C to 1000 °C.

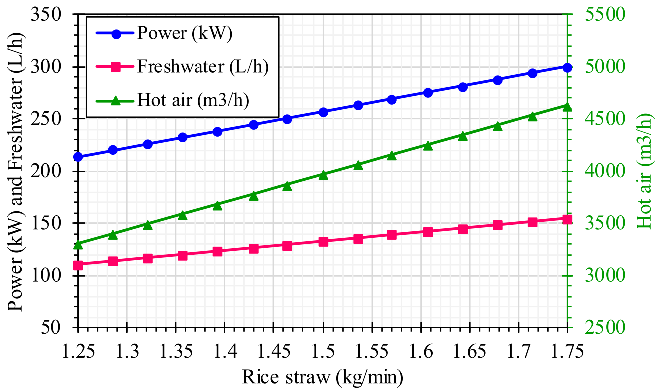

Fig. 12. Variation of power output, freshwater production, and hot air generation with rice straw feed rate, showing increases from 214.1 kW to 299.8 kW (+40.1%), 110.5 L/h to 154.7 L/h (+40.0%), and 3302 m^3/h to 4622 m^3/h (+40.0%) as the biomass feed rises from 1.25 kg/min to 1.75 kg/min.

freshwater production grows from 110.5 L/h to 154.7 L/h, representing a 40.0% enhancement. Similarly, the hot air generation increases from 3302 m^3/h to 4622 m^3/h, amounting to a 40.0% improvement. These nearly proportional increases indicate that the energy conversion processes respond linearly to the available fuel energy within the examined operating range. The observed performance enhancement can be attributed to the larger thermal input provided by higher biomass feed rates. The increased fuel flow results in more syngas production during gasification, which in turn elevates the turbine power output and the availability of exhaust heat for the desalination and air-heating subsystems. Consequently, the multi-generation efficiency of the overall system improves substantially with greater feed availability. However, it is important to note that further increases beyond the studied range could potentially introduce operational challenges such as incomplete combustion, heat exchanger overloading, or reduced turbine performance due to excessive mass flow. Therefore, while a higher feed rate clearly enhances energy and water production capacities, the optimal operating point should balance the benefits of increased output against potential thermodynamic and mechanical constraints.

Fig. 13 presents the effect of rice straw feed rate on the hydrogen (H_2) and oxygen (O_2) storage rates in the integrated hybrid energy system. The results reveal a clear and nearly linear enhancement of both storage parameters as the biomass feed rate increases from 1.25 kg/min to 1.75 kg/min, indicating that the system's electrolysis unit benefits directly from the higher fuel energy input and consequent increase in available electrical power. Quantitatively, the H_2 storage rate rises from 1.57 kg/h to 2.199 kg/h, representing a 40.1% increase, while the O_2 storage rate increases from 12.46 kg/h to 17.45 kg/h, corresponding to a 40.0% improvement. These proportional variations confirm the stoichiometric balance of the water-splitting reaction, where every unit of hydrogen generated is accompanied by a consistent production of oxygen in a fixed molar ratio. The observed trend can be attributed to the higher chemical energy released during biomass gasification at elevated feed rates. The increased production of syngas enhances turbine performance and electricity generation, which in turn supplies more electrical energy to the electrolyzer. As a result, both hydrogen and oxygen generation rates increase steadily with the feed rate. Moreover, the nearly linear relationship between the input biomass rate and the storage capacities suggests efficient energy conversion with minimal system losses within the studied operating range. Increasing the rice straw feed rate significantly improves the hydrogen and oxygen production potential of the system. However, it is essential to maintain optimal feed conditions to prevent excessive fuel consumption or thermal imbalance that could affect long-term system stability and operational efficiency.

Fig. 14 illustrates the influence of rice straw feed rate on the overall system efficiency and emission levels. The feed rate of rice straw was varied between 1.25 kg/min and 1.75 kg/min to evaluate its effect on the performance of the system. Across this entire range, both the efficiency and emission values remained constant, indicating a state of operational stability within the studied interval. Specifically, the system efficiency maintained a constant value of 68.12%, with no observable variation as the rice straw feed rate increased. Similarly, the emission level remained unchanged at 10.68 g/kWh throughout all tested feed rates.

Fig. 15 presents a three-dimensional representation of freshwater production as a function of pressure ratio (PR) and turbine inlet temperature (T) in the proposed multi-generation system. The results indicate a strong dependence of freshwater generation on both operating parameters. At a constant pressure ratio, increasing turbine inlet temperature from 800 to 1000 °C leads to a consistent rise in freshwater production. For instance, at PR = 5, freshwater output increases from 180.9 L/h to 216.8 L/h, while at PR = 15, it rises from 65.98 L/h to 120.9 L/h. This trend can be attributed to the higher thermal energy available in the exhaust gases at elevated temperatures, which enhances the performance of the humidification–dehumidification (HDH) desalination unit. Conversely, at a fixed temperature, increasing the pressure ratio results in a significant reduction in freshwater production. For example, at $T = 800$ °C, freshwater decreases from 180.9 L/h at PR = 5 to 65.98 L/h at PR = 15. This behavior is due to increased energy extraction in the gas turbine at higher pressure ratios, leaving less recoverable heat for desalination.

Fig. 16 presents a three-dimensional representation of overall system efficiency as a function of gas turbine pressure ratio (PR) and turbine

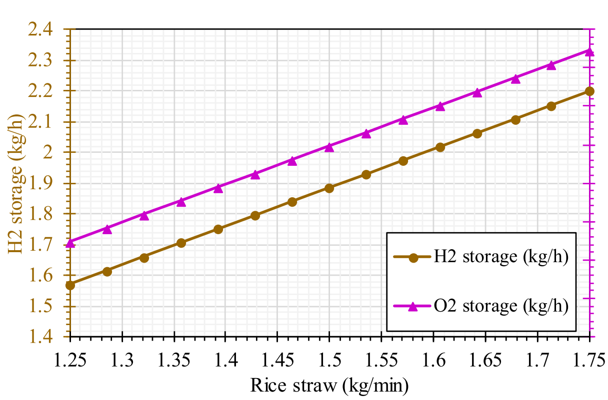

Fig. 13. Variation of hydrogen and oxygen storage rates with rice straw feed rate, showing increases in H_2 storage from 1.57 to 2.199 kg/h (+40.1%) and O_2 storage from 12.46 to 17.45 kg/h (+40.0%) as the feed rate rises from 1.25 kg/min to 1.75 kg/min.

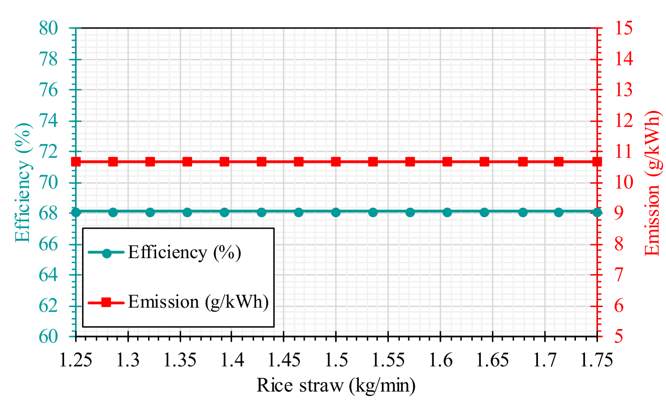

Fig. 14. Variation of system efficiency and emission with respect to rice straw feed rate. Both parameters remain constant across the tested range (1.25–1.75 kg/min), indicating steady-state performance and stable combustion characteristics of the system.

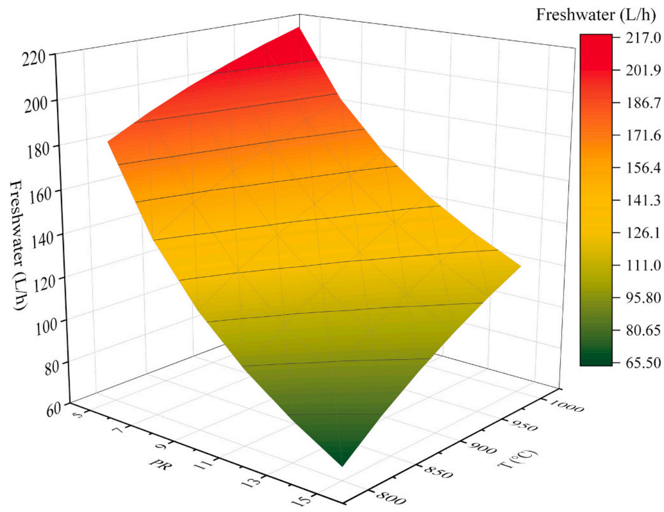

Fig. 15. Three-dimensional variation of freshwater production as a function of gas turbine pressure ratio and turbine inlet temperature in the proposed biomass-based multi-generation system.

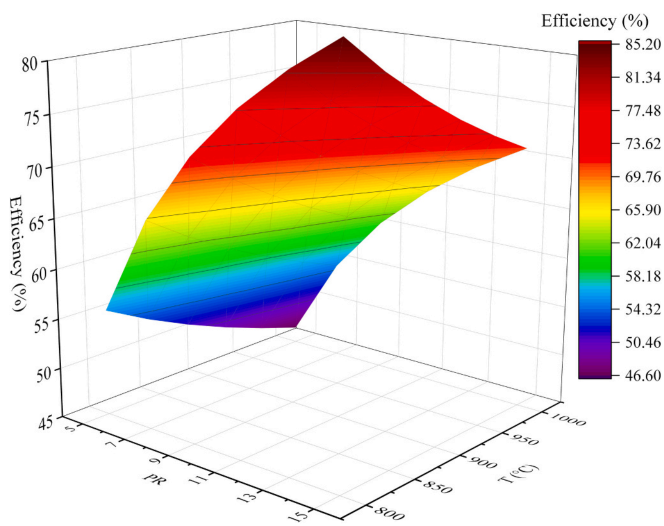

Fig. 16. Three-dimensional variation of overall system efficiency as a function of gas turbine pressure ratio and turbine inlet temperature in the proposed biomass-based multi-generation system.

inlet temperature (T) for the proposed biomass-based multi-generation system. The results reveal two distinct and opposing trends associated with these operating parameters. At a constant pressure ratio, increasing turbine inlet temperature from 800 to 1000 °C leads to a gradual decline in efficiency. For example, at PR = 5, efficiency decreases from 55.64% to 46.61%, while at PR = 15, it drops from 85.08% to 71.17%. This reduction can be attributed to increased thermal losses and a shift toward higher-temperature energy streams that are not fully converted into useful work. In contrast, at a fixed temperature, increasing the pressure ratio significantly enhances system efficiency. At T = 800 °C, efficiency rises from 55.64% at PR = 5 to 85.08% at PR = 15, and a similar trend is observed across all temperature levels. This behavior is primarily due to improved compression and expansion processes in the gas turbine, resulting in more effective energy conversion.

Fig. 17 presents a contour plot illustrating the variation of freshwater production as a function of gas turbine pressure ratio (PR) and rice straw feed rate in the proposed multi-generation system. The contour trends clearly demonstrate that freshwater generation is strongly influenced by both parameters, with opposite effects observed for PR and feed rate. At a constant pressure ratio, increasing the biomass feed rate from 1.25 to 1.75 kg/min results in a nearly linear increase in freshwater production. For instance, at PR = 5, freshwater output rises from 168.1 L/h to 235.3 L/h, while at PR = 15, it increases from 81.63 L/h to 114.3 L/h. This behavior is attributed to the higher thermal energy input associated with greater biomass consumption, which enhances heat recovery for the humidification–dehumidification desalination process. Conversely, at a fixed feed rate, increasing the pressure ratio leads to a consistent reduction in freshwater production. For example, at 1.25 kg/min, freshwater decreases from 168.1 L/h at PR = 5 to 81.63 L/h at PR = 15. This reduction is due to greater energy extraction within the gas turbine cycle, which limits the residual heat available for desalination.

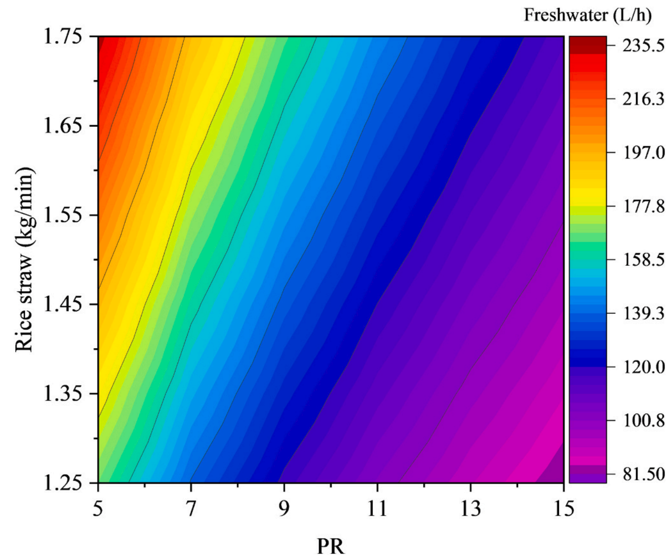

Fig. 17. Contour plot of freshwater production as a function of gas turbine pressure ratio and rice straw feed rate in the proposed biomass-based multi-generation system.

Fig. 18 presents a contour plot illustrating the variation of freshwater production as a function of turbine inlet temperature (T) and rice straw feed rate in the proposed multi-generation system. The results show that freshwater output increases consistently with both increasing

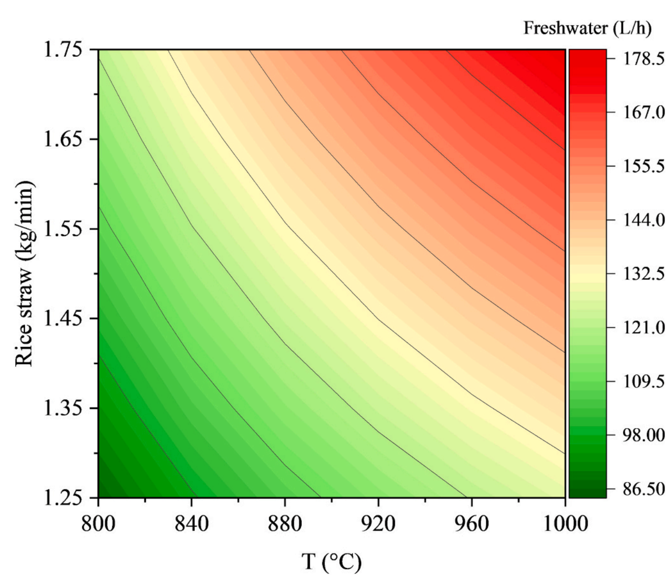

Fig. 18. Contour plot of freshwater production as a function of turbine inlet temperature and rice straw feed rate in the proposed biomass-based multi-generation system.

temperature and biomass feed rate, indicating a synergistic effect of thermal input and fuel supply. At a constant temperature, increasing the rice straw feed rate from 1.25 to 1.75 kg/min leads to a nearly linear rise in freshwater production. For example, at 800 °C, freshwater increases from 86.84 L/h to 121.6 L/h, while at 1000 °C, it grows from 127.5 L/h to 178.5 L/h. This trend reflects the direct impact of higher biomass consumption on the available thermal energy for the humidification–dehumidification desalination process. Similarly, at a fixed feed rate, increasing turbine inlet temperature significantly enhances freshwater generation. At 1.25 kg/min, freshwater rises from 86.84 L/h at 800 °C to 127.5 L/h at 1000 °C, demonstrating the role of elevated exhaust gas temperatures in improving heat recovery and desalination performance.

3.3. Metaheuristic bat algorithm optimization

Fig. 19 presents the optimization results obtained using the metaheuristic bat algorithm, highlighting nine potential optimum points for the integrated multi-generation system. Each point represents a distinct combination of pressure ratio (PR), turbine inlet temperature (T), and rice straw feed rate. The solutions cover a broad operational range: PR varies from 5.04 to 15, T from 800 to 1000 °C, and feed rate from 1.25 to 1.75 kg/min. Notably, several points (e.g., O1, O5, O8) cluster around lower temperatures (800 °C) with moderate PR and feed rates, indicating favorable conditions for balanced energy, hydrogen, and freshwater production. Conversely, points with extreme PR and feed rate values (O2, O3, O6) suggest potential for maximizing specific outputs such as electricity or hydrogen, albeit with trade-offs in efficiency or emissions. The distribution of these points illustrates the flexibility of the system under different operational priorities and demonstrates the effectiveness of the bat algorithm in exploring a multi-dimensional solution space to identify promising candidate configurations for optimal performance.

Fig. 20 illustrates the system outputs corresponding to the nine potential optimum points identified via the metaheuristic bat algorithm. In Fig. 20-a, power, freshwater, and hot-air production are shown. Power ranges from 155.2 kW (O4) to 365.8 kW (O3), indicating that points with higher pressure ratios and feed rates generally achieve greater electricity generation. Freshwater production varies between 64.05 L/h (O2) and 204.72 L/h (O9), showing that lower pressure ratios or higher feed rates favor water yield. Hot air flow spans 2495.8 to 6025.4 m^3/h, with the maximum associated with O9, highlighting trade-offs among outputs. Fig. 20-b presents hydrogen and oxygen storage, where H_2 production ranges from 1.138 kg/h (O4) to 2.683 kg/h (O3), and O_2 storage varies from 9.034 kg/h (O4) to 21.29 kg/h (O3). Points with higher feed rates and moderate PRs favor electrochemical gas production, reflecting enhanced PEM electrolyzer performance. Fig. 20-c shows efficiency and emissions. Efficiency spans 47.12% (O4) to 84.85% (O3), while emissions range from 8.715 g/kWh (O3) to 15.32 g/kWh (O4). This highlights the trade-off between maximizing efficiency and minimizing environmental impact. Overall, O3, O6, and O7 demonstrate high efficiency and acceptable emissions, whereas O4 achieves high freshwater and hot air outputs but at low efficiency and elevated emissions. These results emphasize the multi-objective nature of system optimization and the importance of selecting points that balance all outputs according to operational priorities.

The desirability analysis (based on the equal weights) identifies O7 as the most favorable point with a desirability of 0.653, followed by O6 (0.621) and O3 (0.575). This indicates that O7 provides the best compromise among all objectives, delivering high power, substantial

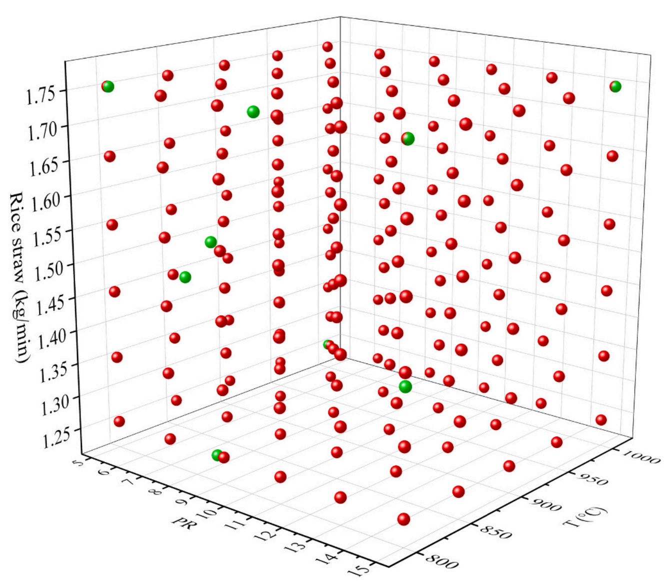

Fig. 19. Optimization results using the metaheuristic bat algorithm, showing nine potential optimum points for the integrated energy system with different combinations of pressure ratio, turbine inlet temperature, and rice straw feed rate.

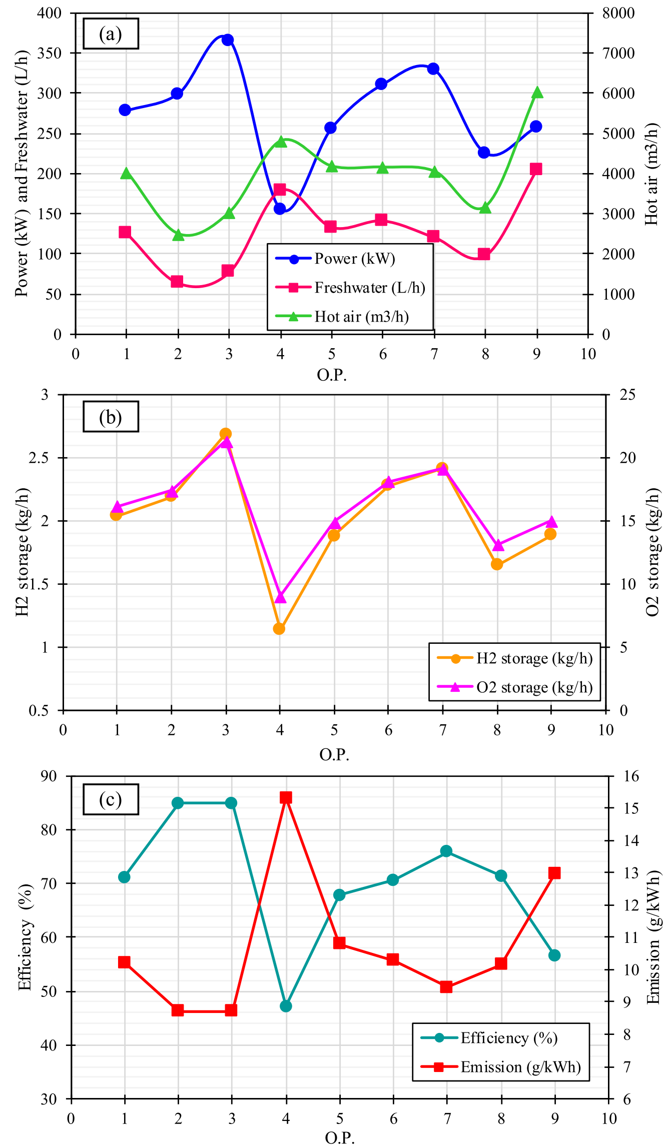

Fig. 20. System outputs at the nine candidate optimum points identified by the bat algorithm: (a) power, freshwater, and hot-air production; (b) hydrogen and oxygen storage; (c) system efficiency and emission rates.

hydrogen and oxygen storage, moderate freshwater and hot-air output, and acceptable efficiency-emission trade-offs. Conversely, O4 has the lowest desirability (0.030), reflecting its poor balance, with low efficiency and high emissions despite high freshwater and hot-air production. These results demonstrate the usefulness of the desirability approach in selecting a truly optimal operational point in a multi-objective system.

Fig. 21 illustrates the schematic performance of the proposed system at the optimal operating point, highlighting the simultaneous generation of electricity, freshwater, hot air, hydrogen, and oxygen together with their corresponding optimal production rates. Under these conditions, it delivers 328.7 kW of power, produces 121.1 L/h of freshwater, supplies 4056.6 m^3/h of hot air, and stores 2.4 kg/h of H_2 and 19.1 kg/h of O_2. The overall efficiency and emissions are 75.8% and 9.5 g/kWh, respectively.

Despite the promising thermodynamic and environmental performance of the proposed multi-generation system, several application challenges should be considered for real-world deployment. The integration of biomass gasification, gas turbine, sCO_2 Brayton cycle, HDH desalination, and PEM electrolysis increases the overall system complexity and requires careful control of heat and mass interactions among the subsystems. In addition, issues such as fluctuations in biomass quality and moisture content, high initial investment cost, material durability under high-temperature and high-pressure conditions, and the need for reliable control strategies may affect stable long-term operation. These practical considerations should be addressed in future pilot-scale and industrial studies to facilitate commercialization of the proposed concept.

Future studies may further extend the present work by investigating off-design and dynamic performance under variable biomass feed conditions and changing energy demands. It would also be valuable to conduct detailed economic, exergoeconomic, and life-cycle assessments to complement the thermodynamic evaluation presented here. In addition, other researchers may explore alternative biomass resources, advanced sCO_2 cycle configurations, improved heat recovery layouts, and hybrid energy-storage strategies to further enhance system flexibility, efficiency, and environmental performance. Experimental validation at pilot scale would also be an important step toward practical implementation.

4. Conclusions

This study investigates a novel biomass-based multi-generation energy system integrating a supercritical CO_2 Brayton cycle, PEM water electrolysis, and HDH desalination for simultaneous production of electricity, hydrogen, oxygen, freshwater, and hot air. The system employs rice straw biomass, leveraging its renewable and carbon-neutral characteristics, and demonstrates significant potential for enhancing energy utilization and reducing environmental impact. Thermodynamic models of all subsystems were validated against literature and experimental data, showing high accuracy and reliability. Performance analyses reveal that increasing the gas turbine pressure ratio enhances electrical power output and hydrogen/oxygen production, while reducing thermal outputs such as freshwater and hot air. Conversely, higher turbine inlet temperatures favor freshwater and hot air generation but slightly decrease power output and electrolyzer performance. Increasing biomass feed rate improves all system outputs proportionally, confirming the importance of fuel availability for maximizing multi-generation efficiency. These trends underscore the necessity of balancing operational parameters to achieve optimal system performance. A key innovation of this research is the application of the metaheuristic bat algorithm for multi-objective optimization. Nine candidate optimum points were identified, demonstrating the flexibility of the system in meeting diverse operational priorities. Desirability analysis highlighted an optimal configuration (O7), achieving a balanced compromise between electrical efficiency, hydrogen/oxygen storage, freshwater and hot air production, and emission levels. This emphasizes the effectiveness of the bat algorithm in navigating the high-dimensional, nonlinear solution space of complex energy systems. The proposed integrated system offers a robust approach for sustainable, efficient, and multi-functional energy generation. By optimizing operational parameters with advanced metaheuristic techniques, the study provides valuable insights for designing next-generation biomass-based energy systems that simultaneously address energy, water, and environmental sustainability goals.

CRediT authorship contribution statement

Yonghui Li: Investigation, Formal analysis. **Ali Basem:** Formal analysis, Data curation. **Hyder H. Abed Balla:** Writing – review &

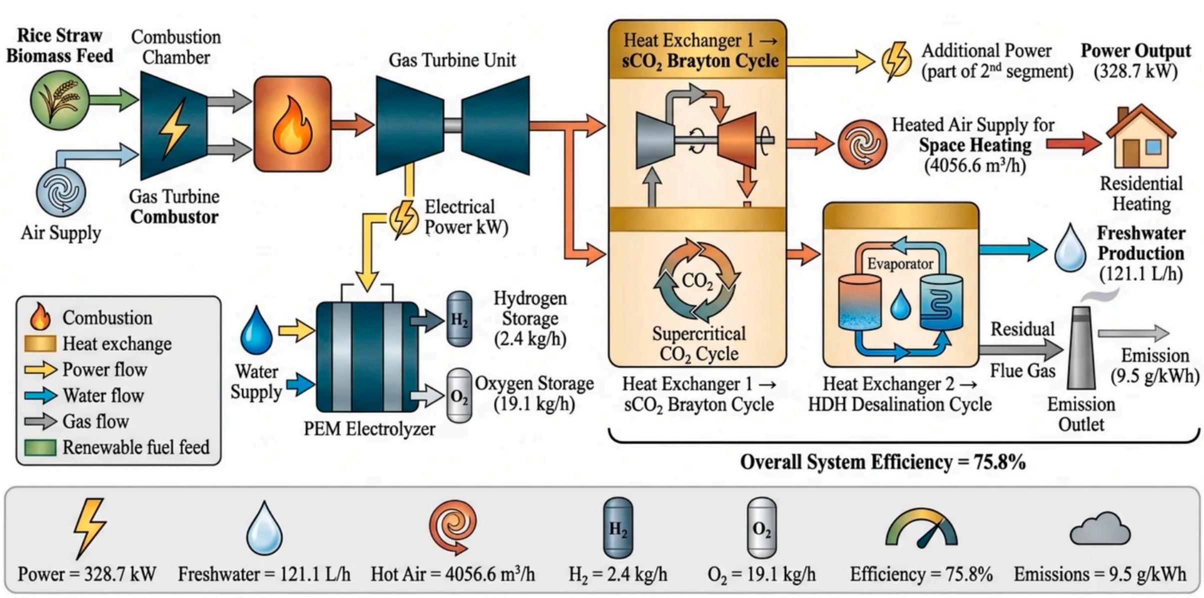

Fig. 21. Schematic representation of the proposed multi-generation energy system operating under optimal conditions, illustrating the integrated production of electricity, freshwater, hot air, hydrogen storage, and oxygen storage along with the corresponding optimal output values.

editing, Supervision, Formal analysis. **Mohamed Arbi Khlifi:** Writing – original draft, Investigation. **Haibo Zhang:** Resources, Formal analysis. **Hanaa Abu-Zinadah:** Writing – review & editing, Validation. **Zainab Ali Bu sinnah:** Methodology, Investigation. **Muyassar Norberdiyeva:** Writing – review & editing, Writing – original draft. **Yasser Fouad:** Supervision, Project administration, Methodology, Conceptualization. **Ibrahim Mahariq:** Validation, Data curation.

Declaration of competing interest

The authors declare that they have no known competing financial interests or personal relationships that could have appeared to influence the work reported in this paper.

Acknowledgement

Ongoing Research Funding program, (ORF-2026-698), King Saud University, Riyadh, Saudi Arabia. This work was financially supported by the Key Project of Philosophy and Social Sciences in Yunnan Province: “Research on Rule Coordination and Governance Innovation in China-Myanmar Cross-Border Data Flow (ZD202525)”; the National Social Science foundation project of China (23BJL088).

Data availability

The authors do not have permission to share data.

References

[1] Zhongkui Zhang, Ling Yao, Khalid Alkhattabi, Omar J. Alkhatib, Ashit Kumar Dutta, Hind Albalawi, H. Elhosiny Ali, Ibrahim Mahariq, A novel biogas combustion-heat recovery for cooling/power co-production system considering a modified sCO2 cycle and a generator-absorber-exchanger (GAX) cycle: machine learning-driven optimization and economic study, Int. Commun. Heat Mass Transfer 174 (2026) 110904.

[2] L. Ji, A. Basem, H.H.A. Balla, O.J. Alkhatib, K. Alkhattabi, Y. Li, I. Mahariq, Integrated wind-solar-LNG system for green liquefied hydrogen and multi-energy supply: techno-economic-environmental analysis and data-driven ANN-GA optimization, Fuel 419 (2026) 138864.

[3] Y. Noorollahi, R. Zahedi, E. Ahmadi, A. Khaledi, Low carbon solar-based sustainable energy system planning for residential buildings, Renew. Sust. Energ. Rev. 207 (2025) 114942.

[4] A.G. Abokhalil, A. Basem, H.H.A. Balla, O.J. Alkhatib, A.S.A. Abood, M. Ayadi, I. Mahariq, Carbon-neutral tri-and multi-generation plants with CO2 capture unit integrated modified gas turbine, recuperative steam Rankine, absorption chiller, and MED: life cycle assessment and multi-scenario chameleon swarm optimization with XGBoost modeling, Appl. Therm. Eng. 290 (2026) 130093.

[5] L. Sun, A. Basem, S. Alhumaid, M. Ayadi, M. Dahari, T. Alharbi, Mahariq, Thermal energy integration and optimization in a biomass-fueled multi-generation system for power, hydrogen, and freshwater production, Case Stud. Therm. Eng. 76 (2025) 107394, https://doi.org/10.1016/j.csite.2025.107394.

[6] P.K. Singh, A. Basem, R.N. Dara, M. Shaban, S. Samad, R. Ghandour, I.A. Alsayer, Waste heat recovery cycles integration into a net-zero emission solar-thermal multi-generation system; techno-economic analysis and ANN-MOPSO optimization, Case Stud. Therm. Eng. 66 (2025) 105690.

[7] P.H. Kumar, N.C. Alluraiah, P. Gopi, M. Bajaj, S. Kumar, C.N.S. Kalyan, V. Blazek, Techno-economic optimization and sensitivity analysis of off-grid hybrid renewable energy systems: a case study for sustainable energy solutions in rural India, Results Eng. 25 (2025) 103674.

[8] N. Chitgar, M. Sadrzadeh, Optimizing sustainable energy systems: A comparative study of geothermal-powered desalination for green hydrogen production, Desalination 593 (2025) 118219.

[9] F. Superchi, A. Bianchini, A. Moustakis, G. Pechlivanoglou, Towards sustainable energy independence: a case study of green hydrogen as seasonal storage integration in a small island, Renew. Energy 245 (2025) 122813.

[10] J. Wang, A. Basem, H.O. Shami, V.A. Musa, P.K. Singh, Y.M. Alanazi, A.S. El-Shafay, A renewable multigeneration system based on biomass gasification and geothermal energy: techno-economic analysis using neural network and Grey wolf optimization, J. Energy Storage 104 (2024) 114519.

[11] Z. Yang, N. Yang, Y. Liu, L. Meng, Y. Shen, R. Kuang, Numerical study on self-sustaining isothermal fermentation in a biogas reactor based on thermal flow-reversal reactor, Intern. Commun. Heat Mass Transf. 174 (2026) 110934.

[12] P. Mojaver, T. Izadi, Development of a smart energy system with energy management for continuous power and heating supply in a hospital through sustainable utilization of internal waste resources, Energy Convers. Manag. 355 (2026) 121267.

[13] D. Sangsefidi, P. Mojaver, Eucalyptus gasification-driven energy system for sustainable hydrogen-rich synthesis gas and energy production: Modeling, analysis, and AI-based multi-objective optimization, Int. J. Hydrog. Energy 216 (2026) 153939.

[14] A. Daneh-Dezfuli, M. Ghanad-Dezfuli, M. Changizian, A novel 4E-based optimization framework for circular biomass multi-generation systems integrating NSGA-II and ANN to enhance resource efficiency and sustainability, Intern. Commun. Heat Mass Transf. 164 (2025) 108849.

[15] E. Karkon, M. Liravi, L. Georges, J. Li, V. Novakovic, Design of a hybrid solar and biomass-based energy system integrated with near-zero energy building: techno-environment investigation and multicriteria optimization, Process Saf. Environ. Prot. 193 (2025) 26–42.

[16] T. Hai, F.M. Alhomayani, P. Ghodratallah, B.S. Chauhan, H. Rajab, S.F. Almojil, A. I. Almohana, Proposal and ANN-assisted optimization of a hybrid solar-and biomass-based energy system for electricity, freshwater, and hydrogen production, Int. J. Hydrog. Energy 107 (2025) 108–122.

[17] D. Pashchenko, R. Mustafin, I. Karpilov, Efficiency of chemically recuperated gas turbine fired with methane: effect of operating parameters, Appl. Therm. Eng. 212 (2022) 118578.

[18] D. Pashchenko, Hydrogen-enriched combustion via exhaust-driven ammonia reforming: a pathway to high-efficiency gas turbine operation, Therm. Sci. Eng. Prog. 67 (2025) 104229, https://doi.org/10.1016/j.tsep.2025.104229.

[19] P. Mojaver, CO2 utilization for H2-rich syngas production in a combined system: bi-objective optimization and machine learning analysis, Energy Convers. Manag. X (2026) 101588.

[20] P. Mojaver, S. Khalilarya, Blue hydrogen production using palladium membrane in a zero-emission energy system by carbon dioxide capturing, Energy 313 (2024) 134142.

[21] D. Pashchenko, Photochemical hydrocarbon fuel regeneration: hydrogen-rich fuel from CO2, Int. J. Hydrog. Energy 47 (61) (2022) 25531–25540.

[22] M. Sharifishourabi, I. Dincer, A. Mohany, A new biomass-solar based energy system with hydrogen production designed for sustainable communities, Energy 336 (2025) 138416, https://doi.org/10.1016/j.energy.2025.138416.

[23] C. Fu, J. Wang, Q. Shen, Z. Cui, S. Ding, Determining the optimal biomass-gasification-based fuel cell trigeneration system in exergy-based cost and carbon footprint method considering energy level, Energy Convers. Manag. 299 (2024) 117802.

[24] W. Xu, J. Zhang, Q. Wu, Y. Wang, W. Zhao, Z. Zhu, P. Cui, Energy, exergy and economic (3E) analyses of a novel DME-power polygeneration system with CO2 capture based on biomass gasification, Appl. Energy 374 (2024) 124031.

[25] H. Chen, S.Q. Salih, A. Almadhor, M.N. Khan, Z. Al Barakeh, R. Ghandour, H. Albalawi, Leveraging multi-effect energy utilization in a biomass-based system for H2 production and urban energy needs: 4E analysis and ANN-based Grey wolf optimization, Energy 333 (2025) 137323.

[26] T. Li, J. Wang, H. Chen, W. Li, P. Pan, L. Wu, H. Chen, Performance analysis of an integrated biomass-to-energy system based on gasification and pyrolysis, Energy Convers. Manag. 287 (2023) 117085.

[27] L. Ju, L. Liu, Y. Han, S. Yang, G. Li, X. Lu, H. Qiao, Robust multi-objective optimal dispatching model for a novel island micro energy grid incorporating biomass waste energy conversion system, desalination and power-to-hydrogen devices, Appl. Energy 343 (2023) 121176.

[28] I. Kayes, R.E. Ratul, A. Abid, F.B. Majmader, Y. Khan, M.M. Ehsan, Multi-objective optimization and 4E (energy, exergy, economy, environmental impact) analysis of a triple cascade refrigeration system, Heliyon 10 (11) (2024).

[29] Y. Wang, G. Xie, A. Rowe, 4E assessment on a CCHP cogeneration Brayton system with dimensional design of PCHEs and turbomachinery, Energy 335 (2025) 138299, https://doi.org/10.1016/j.energy.2025.138299.

[30] L. Zou, Y. Liu, M. Yu, J. Yu, A modified dual-ejector enhanced dual-evaporator transcritical CO2 refrigeration cycle: 4E (energy, exergy, economic and environmental) assessment, Energy Convers. Manag. 303 (2024) 118181.

[31] G. Li, J. Xu, S. Liu, D. Zhao, Y. Zheng, W. Guo, High-energy density micro swirl combustion powered thermoelectric generator for combined heat and power supply, Therm. Sci. Eng. Prog. 68 (2025) 104369.

[32] L. Ye, T. Zheng, X. Wang, X. Liang, C. Liu, Evaluating the heat transfer characteristics of mesh-fed slot cooling configuration: influence of slot height and pin-fin arrangement, Appl. Therm. Eng. 271 (2025) 126304.

[33] L. He, J. Tang, L. Wu, Y. Zhang, H. Mo, Energy consumption optimization of thermal management system for extended-range electric vehicles based on 11-way valve heat pump architecture, Appl. Therm. Eng. 289 (2026) 129529, https://doi.org/10.1016/j.applthermaleng.2025.129529.

[34] S.M. Bouzgarrou, N. Farouk, A.M. Abed, S.A. Khalil, M. Dahari, S. Abdullaev, S. Islam, Harnessing the power of waste in a poly-output system transforming biomass feedstocks into sustainable bio-H2, O2, electricity, and heating, Process. Saf. Environ. Prot. 188 (2024) 177–192.

[35] M. Mehrpooya, M. Khalili, M.M.M. Sharifzadeh, Model development and energy and exergy analysis of the biomass gasification process (based on the various biomass sources), Renew. Sust. Energ. Rev. 91 (2018) 869–887.

[36] H. Zhan, Z. Chen, S. Wang, W. Chen, S. Li, L. Chen, X. Du, A novel hexagonal honeycomb-like geometric-gradient flow field for PEM water electrolyzers, Int. Commun. Heat Mass Transfer 172 (2026) 110597.

[37] R. Yin, B. Chen, L. Sun, Modelica-based multiphysics modeling and multi-timescale dynamic analysis of a 100-kW alkaline water electrolysis system, Renew. Energy 253 (2025) 123620, https://doi.org/10.1016/j.renene.2025.123620.

[38] M. Sheng, H. Rong, C. Zhou, X. Sheng, X. Hu, X. Tang, X. Lu, Simultaneously achieving high energy density, mechanical robustness, and closed-loop

recyclability in phase change materials for advanced thermal energy systems, Adv. Energy Mater. (2026) 70874, https://doi.org/10.1002/aenm.70874.
[39] A.Y. Shash, N.M. Abdeltawab, D.M. Hassan, M. Darweesh, Y.G. Hegazy, Computational methods, artificial intelligence, modeling, and simulation applications in green hydrogen production through water electrolysis: a review, Hydrogen 6 (2) (2025) 21.
[40] K. Kang, C. Cao, C. Jiang, W. Li, C. Tang, Q. Liu, C. Wen, Capacity optimization for minimizing the cost on a hydrogen production system coupling the wind and solar power generation with PEM water electrolysis, Energy 335 (2025) 138076, https://doi.org/10.1016/j.energy.2025.138076.
[41] D. He, H. Li, R. Gao, Y. Li, L. Fan, X. Long, X. Liu, INSL-FLASH: A fission response function based low-cost adaptive reactor physics code for high-Fidelity simulation, Nucl. Sci. Eng. (2025) 1–19.
[42] A. Elmaihy, M.I. Amin, M. Bennaya, A. Rashad, Thermodynamic modeling of alkaline water electrolyzer and assessment of reported cell voltages correlations at low temperature and atmospheric pressure: critical review, J. Energy Storage 96 (2024) 112674.
[43] Y. Zhang, J. Li, M. Yu, X. Chen, X. Chen, J. Shen, Dominant factor identification and fast optimization of Carnot battery by integrating SHAP and physics-guided neural network, Appl. Energy 401 (2025) 126641.
[44] O. Sen, O.F. Guler, C. Yilmaz, M. Kanoglu, Thermodynamic modeling and analysis of a solar and geothermal assisted multi-generation energy system, Energy Convers. Manag. 239 (2021) 114186.
[45] H. Wu, B. Zhang, W. Wang, H. Jin, Optimizing phase equilibrium predictions for the liquefaction of supercritical water gasification products: enhancing energy storage solutions through advanced thermodynamic modeling, Energy 308 (2024) 132845.
[46] K. Hu, J. Fang, X. Ai, D. Huang, Z. Zhong, X. Yang, L. Wang, Comparative study of alkaline water electrolysis, proton exchange membrane water electrolysis and solid oxide electrolysis through multiphysics modeling, Appl. Energy 312 (2022) 118788.
[47] R. Cao, Y. Wang, W. Li, H. Ni, Y. Duan, Thermodynamics analysis of a hybrid system based on a combination of hydrogen fueled compressed air energy storage system and water electrolysis hydrogen generator, Int. J. Hydrog. Energy 48 (63) (2023) 24492–24503.
[48] A.M. Al-Mahgari, A. Moh'd, A. N, S.A. Khashan, Pressurized green hydrogen from water electrolysis: compression before or after electrolysis? A comparison among different configurations, J. Energy Storage 73 (2023) 109251.
[49] M. Nasser, H. Hassan, Assessment of hydrogen production from waste heat using hybrid systems of Rankine cycle with proton exchange membrane/solid oxide electrolyzer, Int. J. Hydrog. Energy 48 (20) (2023) 7135–7153.
[50] L. Peng, T.R. Alsenani, M. Li, H. Lin, H.N. Sabeh, F. Alturise, S.B.H. Hassine, Using data-driven learning methodology for a solid waste-to-energy scheme and developed regression analyses for performance prediction, Process Saf. Environ. Prot. 178 (2023) 622–641.
[51] N. Sezer, S. Bayhan, U. Fesli, A. Sanfilippo, A comprehensive review of the state-of-the-art of proton exchange membrane water electrolysis, Mater. Sci. Energy Technol. 8 (2025) 44–65.
[52] W. Tao, L. Xiangyang, H. Maogang, Investigation on the bond-breaking of lignin and the mechanism of lignin gasification in supercritical carbon dioxide and supercritical water, Biomass Bioenergy 194 (2025) 107630.
[53] Z. Gong, Y. Zou, S. Cheng, B. Tan, P. Zhao, A review of research on liquid-metal-cooled reactor and supercritical carbon dioxide Brayton cycle coupled system, Prog. Nucl. Energy 190 (2026) 105957.
[54] G. Manente, A. Lazzaretto, Innovative biomass to power conversion systems based on cascaded supercritical CO2 Brayton cycles, Biomass Bioenergy 69 (2014) 155–168.
[55] Z. Huang, H. You, J. Han, G. Li, Y. Xiao, B. Hu, D. Chen, Techno-economic evaluation and multi-objective optimization of a cogeneration system integrating solid oxide fuel cell with steam Rankine and supercritical carbon dioxide Brayton cycles, Fuel 382 (2025) 133675.
[56] K.Q. Chen, W.H. Pu, Q. Zhang, B.S. Lan, Z.Y. Song, Y.Q. Mao, Thermal performance analysis on steady-state and dynamic response characteristic in solar tower power plant based on supercritical carbon dioxide Brayton cycle, Energy Sources, Part A 47 (1) (2025) 1927–1949.
[57] C. Dong, G. He, Z. Meng, S. Asim, D. Li, Y. Hu, Optimality criterion-based latent heat storage heat exchangers topology optimization method, J. Energy Storage 125 (2025) 117012.
[58] K. Cheng, J. Yu, C. Dang, J. Qin, W. Jing, Performance comparison between closed-Brayton-cycle power generation systems using supercritical carbon dioxide and helium–xenon mixture at ultra-high turbine inlet temperatures on hypersonic vehicles, Energy 293 (2024) 130653.
[59] M. Das, K.S. Reddy, Modelling and optimization of combined supercritical carbon dioxide Brayton cycle and organic Rankine cycle for electricity and hydrogen production, Appl. Energy 377 (2025) 124586.
[60] G. Xia, X. He, Y. Jia, Y. Zhu, Z. Tian, Design of a cylindrical thermal rotary concentrator based on transformation thermodynamics, Materials 18 (19) (2025) 4440.
[61] Z. Liu, P. Wang, X. Sun, B. Zhao, Analysis on thermodynamic and economic performances of supercritical carbon dioxide Brayton cycle with the dynamic component models and constraint conditions, Energy 240 (2022) 122792.
[62] B. Zhang, Y. Xue, Y. Zhang, K. Su, A self-calibrating digital twin for space thermionic nuclear reactors under fault conditions, Reliab. Eng. Syst. Saf. 268 (2025) 111995, https://doi.org/10.1016/j.ress.2025.111995.
[63] G. Soyturk, O. Kizilkan, Modeling and analysis of solid oxide fuel cell-based multigeneration system with supercritical and transcritical carbon dioxide power cycles, humidification-dehumidification system and hydrogen generation, Energy Convers. Manag. 332 (2025) 119762.
[64] L. Ye, H. Guo, Y. Zhu, P. Jiang, Large eddy simulation of film cooling flow from diffusion slot hole with crossflow coolant configuration, Phys. Fluids 35 (5) (2023).
[65] A. Chitsaz, S. Khalilarya, P. Mojaver, Supercritical CO2 utilization in a CO2 zero emission novel system for bio-synthetic natural gas, power and freshwater productions, J. CO_2 Util. 59 (2022) 101947.
[66] D. Kong, X. Tian, G. Li, C. Liu, X. Niu, S.A. Isaev, O.G. Penyazkov, Numerical study of particle deposition and heat transfer characteristics in an S-shaped miniature cooling channel of a gas turbine blade, Powder Technol 468 (2025) 121612, https://doi.org/10.1016/j.powtec.2025.121612.
[67] I. Tlili, M. Osman, E.M. Barhoumi, I. Alarifi, A.G. Abo-Khalil, R.P. Praveen, K. Sayed, Performance enhancement of a humidification–dehumidification desalination system: A thermodynamic investigation, J. Therm. Anal. Calorim. 140 (1) (2020) 309–319.
[68] M. Alrbai, A. Al Masri, D. Makawii, A. Alahmer, Optimizing humidification–dehumidification desalination systems: impact of nozzle position and geometric configuration on performance and efficiency, Intern. J. Thermof. 26 (2025) 101117.
[69] M.R.A. Malek, N.A.A. Aziz, S. Alelyani, M. Mohana, F.N.A. Baharudin, Z. Ibrahim, Comfort and energy consumption optimization in smart homes using bat algorithm with inertia weight, J. Build. Eng. 47 (2022) 103848.
[70] M. Capocelli, M. Balsamo, L. Mazzeo, M. Luberti, Thermodynamic analysis of the humidification-dehumidification-adsorption (HDHA) desalination process, Desalination 554 (2023) 116510.
[71] K. Guerraiche, L. Dekhici, E. Chatelet, A. Zeblah, Multi-objective electrical power system design optimization using a modified bat algorithm, Energies 14 (13) (2021) 3956.
[72] Z.A.A. Alyasseri, O.A. Alomari, M.A. Al-Betar, S.N. Makhadmeh, I.A. Doush, M. A. Awadallah, A. Elnagar, Recent advances of bat-inspired algorithm, its versions and applications, Neural Comput. & Applic. 34 (19) (2022) 16387–16422.
[73] X. Hu, W. Jiang, X. Ying, M. Eslami, The application of a new design of bat optimizer for energy efficiency enhancement in PEMFCs based on fractional order theory, Sustain. Energy Techn. and Assess. 55 (2023) 102904.
[74] W.H. Zhou, Y.X. Wu, Y. Zhao, J. Xu, Research on multi-energy complementary microgrid scheduling strategy based on improved bat algorithm, Energy Rep. 8 (2022) 1258–1272.
[75] S. Chen, A. Slowik, Y. Chen, Y.H. She, X.S. He, Quantum-computing-driven bat algorithm: balancing exploration-exploitation with predictive mutation and frequency adjustment for optimization, Expert Syst. Appl. 283 (2025) 127714, https://doi.org/10.1016/j.eswa.2025.127714.
[76] H. Rostamzadeh, A.S. Namin, H. Ghaebi, M. Amidpour, Performance assessment and optimization of a humidification dehumidification (HDH) system driven by absorption-compression heat pump cycle, Desalination 447 (2018) 84–101.
[77] T. Ioroi, K. Yasuda, Z. Siroma, N. Fujiwara, Y. Miyazaki, Thin film electrocatalyst layer for unitized regenerative polymer electrolyte fuel cells, J. Power Sources 112 (2) (2002) 583–587.
[78] P. Ahmadi, I. Dincer, M.A. Rosen, Energy and exergy analyses of hydrogen production via solar-boosted ocean thermal energy conversion and PEM electrolysis, Int. J. Hydrog. Energy 38 (4) (2013) 1795–1805.
[79] J. Sarkar, S. Bhattacharyya, Optimization of recompression S-CO2 power cycle with reheating, Energy Convers. Manag. 50 (8) (2009) 1939–1945.
[80] T.K. Ibrahim, M.M. Rahman, A.N. Abdalla, Gas turbine configuration for improving the performance of combined cycle power plant, Procedia Eng. 15 (2011) 4216–4223.
[81] Z. Ghaffarpour, M. Mahmoudi, A.H. Mosaffa, L.G. Farshi, Thermoeconomic assessment of a novel integrated biomass based power generation system including gas turbine cycle, solid oxide fuel cell and Rankine cycle, Energy Convers. Manag. 161 (2018) 1–12.
[82] P. Ahmadi, S. Khanmohammadi, F. Musharavati, M. Afrand, Development, evaluation, and multi-objective optimization of a multi-effect desalination unit integrated with a gas turbine plant, Appl. Therm. Eng. 176 (2020) 115414.
[83] Y. Haseli, I. Dincer, G.F. Naterer, Thermodynamic analysis of a combined gas turbine power system with a solid oxide fuel cell through exergy, Thermochim. Acta 480 (1–2) (2008) 1–9.
[84] M. Ebrahimi, S. Majidi, Exergy-energy-environ evaluation of combined cooling heating and power system based on a double stage compression regenerative gas turbine in large scales, Energy Convers. Manag. 150 (2017) 122–133.
[85] P. Mojaver, S. Jafarmadar, S. Khalilarya, A. Chitsaz, Investigation and optimization of a co-generation plant integrated of gasifier, gas turbine and heat pipes using minimization of Gibbs free energy, Lagrange method and response surface methodology, Int. J. Hydrog. Energy 45 (38) (2020) 19027–19044.
[86] Sanjay, O. Singh, B.N. Prasad, Thermodynamic performance of complex gas turbine cycles, in: International Joint Power Generation Conference vol. 36177, 2002, January, pp. 529–535.
[87] A.O. Bakare, A. Nasir, O.R. Abiodun, S. Bako, Combined Cycle Gas Turbine: Operation and Performance Analysis, in: Proceedings of the 1st AGM and Conference of the Nigerian Institution of Mechanical Engineers, 2016, September, pp. 57–68.
[88] T.K. Ibrahim, M.M. Rahman, Optimum performance improvements of the combined cycle based on an intercooler–reheated gas turbine, J. Energy Resour. Technol. 137 (6) (2015) 061601.
[89] E. Assareh, A. Ershadi, M. Lee, An integrated system for producing electricity and fresh water from a new gas-fired power plant and a concentrated solar power plant–case study–(Australia, Spain, South Korea, Iran), Renew. Energy Focus 44 (2023) 19–39.

[90] P. Ding, X. Liu, H. Qi, H. Shen, X. Liu, S.G. Farkoush, Multi-objective optimization of a new cogeneration system driven by gas turbine cycle for power and freshwater production, J. Clean. Prod. 288 (2021) 125639.
[91] F. Yilmaz, M. Ozturk, R. Selbas, Design and thermodynamic assessment of a biomass gasification plant integrated with Brayton cycle and solid oxide steam electrolyzer for compressed hydrogen production, Int. J. Hydrog. Energy 45 (60) (2020) 34620–34636.
[92] M. Abid, M.S. Khan, T.A.H. Ratlamwala, Comparative energy, exergy and exergo-economic analysis of solar driven supercritical carbon dioxide power and hydrogen generation cycle, Int. J. Hydrog. Energy 45 (9) (2020) 5653–5667.
[93] T. Hai, M.A. Ali, A.A. Alizadeh, S.F. Almojil, A.I. Almohana, B.S. Chauhan, A. Raise, Optimization next to environmental analysis of harvesting waste heat from a biomass-driven externally-fired gas turbine cycle for sub-zero cooling and production of hydrogen, freshwater, and hot water, Appl. Therm. Eng. 223 (2023) 119884.